



**Adailton José do Nascimento Sousa**

**Dimensionless Ensemble Smoother With  
Multiple Data assimilation applied on an  
Inverse Problem of a multilayer reservoir with a  
damaged zone.**

**Dissertação de Mestrado**

Thesis presented to the Programa de Pós-graduação em Matemática, do Departamento de Matemática da PUC-Rio in partial fulfillment of the requirements for the degree of Mestre em Matemática.

Advisor : Prof. Sinesio Pesco  
Co-advisor: Dr. Renan Vieira Bela

Rio de Janeiro  
October 2022



**Adailton José do Nascimento Sousa**

**Dimensionless Ensemble Smoother With  
Multiple Data assimilation applied on an  
Inverse Problem of a multilayer reservoir with a  
damaged zone.**

Thesis presented to the Programa de Pós-graduação em Matemática da PUC-Rio in partial fulfillment of the requirements for the degree of Mestre em Matemática. Approved by the Examination Committee:

**Prof. Sinesio Pesco**

Advisor

Departamento de Matemática – PUC-Rio

**Dr. Renan Vieira Bela**

Co-advisor

Transportadora Brasileira Gasoduto Bolívia-Brasil S.A.

**Prof. Alexandre Anozé Emerick**

Petróleo Brasileiro - Rio de Janeiro - Matriz

**Prof. Marcio da Silveira Carvalho**

Departamento de Engenharia Mecânica – PUC-Rio

**Dr. Thiago de Menezes Duarte e Silva**

Departamento de Matemática – PUC-Rio

**Prof. Abelardo Borges Barreto Jr**

Departamento de Matemática – PUC-Rio

Rio de Janeiro, October 11th, 2022

All rights reserved.

**Adailton José do Nascimento Sousa**

Graduated in Mathematics by PUC-Rio.

Bibliographic data

Sousa, Adailton José do Nascimento

Dimensionless Ensemble Smoother With Multiple Data assimilation applied on an Inverse Problem of a multilayer reservoir with a damaged zone. / Adailton José do Nascimento Sousa; advisor: Sinesio Pesco; co-advisor: Renan Vieira Bela. – 2022.

69 f: il. color. ; 30 cm

Dissertação (mestrado) - Pontifícia Universidade Católica do Rio de Janeiro, Departamento de Matemática, 2022.

Inclui bibliografia

1. Matemática – Teses. 2. Ensemble smoother com múltipla assimilação de dados. 3. Teste de injetividade. 4. Zona de Skin. 5. Estimativa de Parâmetros. I. Pesco, Sinesio. II. R.V. Bela. III. Pontifícia Universidade Católica do Rio de Janeiro. Departamento de Matemática. IV. Título.

CDD: 004

To my mom,  
To my future wife Mônica,  
To all my friends,  
Specially Jéssica and Matheus  
for their support and encouragement.

## Acknowledgments

To my advisor, Professor Sinesio Pesco, for the stimulus, encouragement, and belief in myself even when I lost faith on myself.

To Professor Abelardo, Thiago, Renan, for the patience to explain this area.

To all the members of the Mathematical department, especially Creuza, Mariana and Katia.

To my best friends, Jéssica and Matheus, for all advices especially when I was not okay.

To my mom, Raimunda, one of the most important person on my life and a lot of time the reason I did not give up.

To my future wife, Mônica. I hope one day to repay all the love, patience and good you have given me.

This study was financed in part by the Coordenação de Aperfeiçoamento de Pessoal de Nível Superior - Brasil (CAPES) - Finance Code 001

I want to thank PETROBRAS and PUC-Rio for their support in this project.

## Abstract

Sousa, Adailton José do Nascimento; Pesco, Sinesio (Advisor); R.V. Bela (Co-Advisor). **Dimensionless Ensemble Smoother With Multiple Data assimilation applied on an Inverse Problem of a multilayer reservoir with a damaged zone.** Rio de Janeiro, 2022. 69p. Dissertação de Mestrado – Departamento de Matemática, Pontifícia Universidade Católica do Rio de Janeiro.

The ES-MDA has been extensively used concerning inverse problems of oil reservoirs, using Bayesian statistics as the core. Important properties such as permeability, skin zone radius, and skin zone permeability are estimated from historical reservoir data using this set-based method. In this thesis, the pressure measured at the well during an injectivity test was calculated using an analytical approach of a multilayer reservoir, with skin zone, using the Laplace Transform. Stehfest's algorithm was used to invert the data to the real field. Furthermore, using this approach, we were able to easily obtain the flow rate in each layer as new data to be considered in the ES-MDA, enriching the estimation of the targeted data. As we use flow rate and pressure as input data in the ES-MDA, it is important to assure that the difference in orders of magnitude does not influence our estimates. For this reason, we chose to use the ES-MDA in the dimensionless form. Aiming at a greater precision of our estimates, we used an algorithm to optimize the ES-MDA inflation factors.

## Keywords

Ensemble smoother with multiple data assimilation; Injectivity Test; Skin zone; Parameter Estimation .

## Resumo

Sousa, Adailton José do Nascimento; Pesco, Sinesio; R.V. Bela. **Ensemble Smoother adimensional com múltipla assimilação aplicado a um problema Inverso de reservatório multicamadas com zona de skin.** Rio de Janeiro, 2022. 69p. Dissertação de Mestrado – Departamento de Matemática, Pontifícia Universidade Católica do Rio de Janeiro.

O ES-MDA tem sido usado amplamente no que diz respeito a problemas inversos de reservatórios de petróleo, usando a estatística bayesiana como cerne. Propriedades importantes como a permeabilidade, raio da zona de skin e permeabilidade da zona de skin, são estimadas a partir de dados de histórico de reservatório usando esse método baseado em conjuntos. Nessa tese, a pressão medida no poço durante um teste de injetividade foi calculada usando uma abordagem analítica de um reservatório multicamadas, com zona de skin, usando a Transformada de Laplace. O algoritmo de Stehfest foi usado para inverter os dados para o campo real. Além disso, ao usarmos essa abordagem, conseguimos obter facilmente a vazão em cada camada como um novo dado a ser considerado no ES-MDA, enriquecendo a estimativa dos dados desejados. Por usarmos a vazão e a pressão como dados de entrada no ES-MDA, é de suma importância que a diferença de ordens de grandezas não influencie em nossas estimativas e por isso optou-se por usar o ES-MDA na forma adimensional. Visando uma maior precisão de nossas estimativas, usou-se um algoritmo de otimização dos fatores de inflação do ES-MDA.

## Palavras-chave

Ensemble smoother com múltipla assimilação de dados; Teste de injetividade; Zona de Skin; Estimativa de Parâmetros.

## Table of contents

|          |                                    |           |
|----------|------------------------------------|-----------|
| <b>1</b> | <b>Introduction</b>                | <b>12</b> |
| <b>2</b> | <b>Mathematical Model</b>          | <b>14</b> |
| 2.1      | Reservoir Model                    | 14        |
| 2.2      | Modeling the solution              | 15        |
| <b>3</b> | <b>Ensemble-Based Methods</b>      | <b>29</b> |
| 3.1      | Bayesian Statistics                | 29        |
| 3.2      | Ensemble Smoother                  | 32        |
| 3.3      | Inflation Factors Analysis         | 36        |
| <b>4</b> | <b>Results</b>                     | <b>43</b> |
| 4.1      | Proposed Methodology               | 43        |
| 4.2      | Case A                             | 45        |
| 4.3      | Case B                             | 49        |
| 4.4      | Case C                             | 53        |
| 4.5      | Case D                             | 60        |
| <b>5</b> | <b>Conclusion and Future Works</b> | <b>65</b> |
| <b>6</b> | <b>Bibliography</b>                | <b>67</b> |

## List of figures

|             |  |    |
|-------------|--|----|
| Figure 2.1  | Reservoir Model  | 14 |
| Figure 2.2  | Configuration for $r_F > r_s$                                    | 16 |
| Figure 2.3  | Configuration for $r_F < r_s$                                    | 16 |
| Figure 4.1  | Pressure response for case A                                     | 46 |
| Figure 4.2  | Flow-Rate response on layer 1 for case A                         | 46 |
| Figure 4.3  | Permeability of the damaged zone histogram on layer 1 for case A | 47 |
| Figure 4.4  | Permeability of the damaged zone histogram on layer 2 for case A | 47 |
| Figure 4.5  | Radius of the damaged zone histogram on layer 1 for case A       | 48 |
| Figure 4.6  | Radius of the damaged zone histogram on layer 2 for case A       | 48 |
| Figure 4.7  | Permeability histogram on layer 1 for case A                     | 48 |
| Figure 4.8  | Permeability histogram on layer 2 for case A                     | 49 |
| Figure 4.9  | Pressure response for case B                                     | 50 |
| Figure 4.10 | Flow-Rate response on layer 1 for case B                         | 50 |
| Figure 4.11 | Permeability of the damaged zone histogram on layer 1 for case B | 51 |
| Figure 4.12 | Permeability of the damaged zone histogram on layer 2 for case B | 51 |
| Figure 4.13 | Radius of the damaged zone histogram on layer 1 for case B       | 52 |
| Figure 4.14 | Radius of the damaged zone histogram on layer 2 for case B       | 52 |
| Figure 4.15 | Permeability histogram on layer 1 for case B                     | 53 |
| Figure 4.16 | Permeability histogram on layer 2 for case B                     | 53 |
| Figure 4.17 | Pressure response for case C                                     | 54 |
| Figure 4.18 | Flow-Rate response on layer 1 for case C                         | 54 |
| Figure 4.19 | Flow-Rate response on layer 2 for case C                         | 55 |
| Figure 4.20 | Permeability of the damaged zone histogram on layer 1 for case C | 56 |
| Figure 4.21 | Permeability of the damaged zone histogram on layer 2 for case C | 56 |
| Figure 4.22 | Permeability of the damaged zone histogram on layer 3 for case C | 57 |
| Figure 4.23 | Radius of the damaged zone histogram on layer 1 for case C       | 57 |
| Figure 4.24 | Radius of the damaged zone histogram on layer 2 for case C       | 58 |
| Figure 4.25 | Radius of the damaged zone histogram on layer 3 for case C       | 58 |
| Figure 4.26 | Permeability histogram on layer 1 for case C                     | 59 |
| Figure 4.27 | Permeability histogram on layer 2 for case C                     | 59 |
| Figure 4.28 | Permeability histogram on layer 3 for case C                     | 60 |
| Figure 4.29 | Pressure response for case D                                     | 60 |
| Figure 4.30 | Flow-Rate response on layer 1 for case D                         | 61 |
| Figure 4.31 | Permeability of the damaged zone histogram on layer 1 for case D | 62 |
| Figure 4.32 | Permeability of the damaged zone histogram on layer 2 for case D | 62 |

|             |  |    |
|-------------|--|----|
| Figure 4.33 | Radius of the damaged zone histogram on layer 1 for case D | 63 |
| Figure 4.34 | Radius of the damaged zone histogram on layer 2 for case D | 63 |
| Figure 4.35 | Permeability histogram on layer 1 for case D               | 64 |
| Figure 4.36 | Permeability histogram on layer 2 for case D               | 64 |

## List of tables

|           |                                |    |
|-----------|--------------------------------|----|
| Table 4.1 | Table for Input parameters     | 44 |
| Table 4.2 | Table for all Cases Properties | 45 |

# 1

## Introduction

The study of injectivity tests has been influential in petroleum reservoir characterization. However, the determination of individual layer properties on multilayer reservoirs remains a challenging task. Primarily due to the high non-linearity of the problem. Due to its importance, some mathematical formulations were developed to determine the pressure difference in injectivity tests.

(BARRETO; PERES; PIRES, 2011) presents a perspective of calculating the pressure difference on the real field; (NETO et al., 2020) presents a study for three regions reservoirs, but only with one layer using an approach of the Laplace domain. (MASTBAUM et al., 2021) use the same proposal and present good results for reservoirs with two layers, extending this model to the case with two regions. Also, (VIANA et al., 2022) presented a case considering a reservoir with an arbitrary number of layers and regions, considering the cross-flow, but with no damaged zone

The works that use an approach of results on the Laplace domain invert their outcomes to the real field by the Stehfest algorithm (STEHFEST, 1970). The problem studied in this thesis is an injectivity test, considering the skin zone properties in a reservoir with an arbitrary number of layers. Therefore, we consider a multilayer reservoir model with three regions.

Some advantages of using an analytical approach are the possibility of obtaining asymptotic approximations and identifying characteristic signatures and the ease compared to a numerical simulator. Furthermore, our characterization approach uses the pressure and each layer's liquid rate data, obtaining a robust reservoir characterization. Thus, the piston-like water displacement assumption might not hinder the proposed characterization procedure.

We could quickly calculate the flow-rate in the Laplace domain with pressure data. We needed to derive the pressure and obtain the flow rate, launching the possibility of using it as another data to consider to estimate the reservoir properties, which could increase the accuracy of estimative of the parameters.

Also, using the differential equations for both phases in the reservoir layers, it was possible to set up a system of linear equations to determine the pressure difference in the Laplace field. Moreover, using the Stehfest algorithm (STEHFEST, 1970), it was possible to invert the solution and the flow-rate to the real domain.

A classical approach to solving optimization problems is the use of gradient-based algorithms. Nevertheless, this kind of method has a substantial computational cost. An alternative that has been broadly used is ensemble-based methods. Since this kind of method use statistic for estimating derivatives, they do not need to calculate the gradient vector.

This thesis creates the initial ensemble using a normal distribution for all estimated parameters and uses the method to estimate a final ensemble for the parameters, fitting the observed data. We used the dimensionless ensemble smoother with multiple data assimilation (ZHANG; REYNOLDS; OLIVER, 2002) in this work due to the difference in magnitude of the data.

In this thesis, we consider piston-like water displacement. As a result, we lose little accuracy when computing the dynamic data. However, we can obtain the liquid rate in each layer, which might enhance reservoir properties estimation in a history-matching methodology. Comparing our technique with the one proposed by (SILVA et al., 2021), we may obtain a more precise characterization of each reservoir layer's properties due to the insertion of one more rich data corresponding to that specific layer.

Four different cases were presented, similar to the study of (SILVA et al., 2021), trying to verify how it works for the different scenarios. For each case, we estimated all layers' permeability, radius, and permeability for the damaged zone and aimed to fit the observed pressure difference data and flow rate data. The main objective of this work is to extend the work of (SILVA et al., 2021), including the flow-rate as data, but expanding the number of parameters to be estimated, increasing the complexity of the problem.

This dissertation is divided into four chapters. Chapter 2 presents the model to obtain the flow-rate and pressure difference responses. Chapter 3 uses the Dimensionless Ensemble Smoother with Multiple Data Assimilation to estimate reservoir properties, which utilizes the flow-rate and pressure difference as data. The results for four different cases were presented in chapter 4, and finally, chapter 5 exhibits the conclusion.

## 2 Mathematical Model

In this chapter, we aim to explain the mathematical model used to obtain pressure difference and flow-rate data. We first focus on the kind of reservoir studied, then model the problem's solution, using all restrictions.

The data obtained here is used later in Chapter 3 as input for the statistic method applied. Also, it is possible to obtain the flow-rate after evaluating the pressure difference in the Laplace Domain.

### 2.1 Reservoir Model

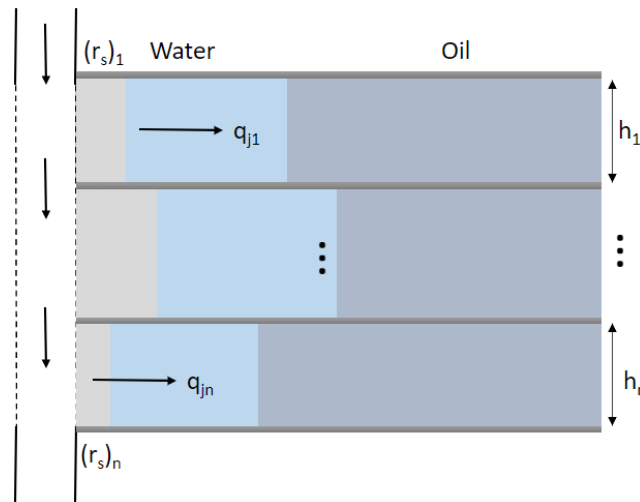


Figure 2.1: Reservoir Model

Figure 2.1 illustrates the reservoir model studied. An arbitrary number  $n$  of layers are supposed, and each has distinct properties. Since a damaged zone is considered, each layer will have three regions, one with properties of the aqueous phase, the other with oil properties, and the region of the damaged zone.

The following hypotheses are considered to build the formulation:

1. Constant thickness at each layer ( $h_j$ )
2. Constant flow-rate during injection time
3. Constant initial pressure in all layers and small pressure gradients.

4. Flow-rate is isothermal, with negligible gravitational forces and rejecting the impact of capillary forces
5. Oil properties are the same in all layers
6. Fluids behave are slightly compressible with constant viscosity.
7. A stratified reservoir
8. A piston-like water displacement

## 2.2

### Modeling the solution

The condition that Each region has independent properties is presumed. The waterfront radius ( $r_F$ ) for the  $j$ th layer is calculated using the formulation (BUCKLEY; LEVERETT, 1942):

$$r_{Fj} = \sqrt{r_w^2 + \frac{\int_0^t q_j d\tau}{24\pi\phi_j h_j} f'_w t} \quad (2-1)$$

Considering a piston water displacement, it is known (NETO et al., 2020) that  $f'_w = \frac{1}{1 - S_{or} - S_{wi}}$ .

Defining the hydraulic diffusivity ( $\eta_j$ ) and fluid mobility ( $\hat{\lambda}_j$ ) for the  $j$ th layer for both damaged and reservoir zone as in (NETO et al., 2020):

In the damaged zone:

$$\eta_{fs_j} = \frac{k_{s_j} k_{rf_j}}{\phi \mu_f c_t} \text{ and } \hat{\lambda}_{fs_j} = \frac{k_{s_j} k_{rf}}{\mu_f} \text{ with } f = w, o. \quad (2-2)$$

In the reservoir zone:

$$\eta_{fR_j} = \frac{k_j k_{rf_j}}{\phi \mu_f c_t} \text{ and } \hat{\lambda}_{fR_j} = \frac{k_j k_{rf}}{\mu_f} \text{ with } f = w, o. \quad (2-3)$$

As a result, there are two possible configurations:

1. The waterfront radius has overtaken the damaged zone (Figure 2.2)
2. The waterfront radius is within the damaged zone (Figure 2.3)

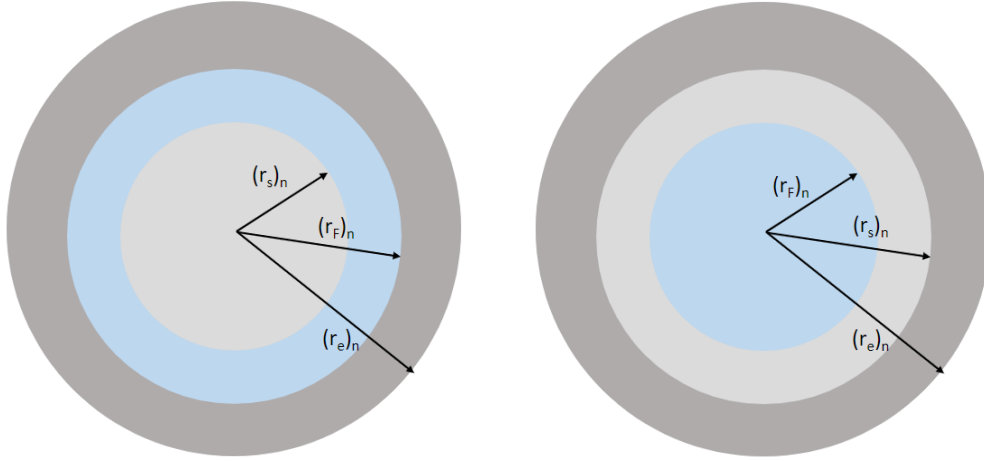


Figure 2.2: Configuration for  $r_F > r_s$  Figure 2.3: Configuration for  $r_F < r_s$

Focusing on the configuration where  $r_F < r_s$  and aiming at the solution of the system, the properties of each region and fluid within must be considered, as well as the diffusivity equation for fluids with low compressibility. On an arbitrary layer where the waterfront is within the damaged area, the conditions led to certain equations on the respective regions, each one reflecting a specific feature:

- The initial condition (IC) specifies the pressure distribution before the water injection starts.
- The external boundary condition (EBC) reflects the conditions at the extreme of the reservoir. A radially infinite reservoir is considered.
- The internal boundary condition (IBC) corresponds to how the water is injected during the test.
- Coupling Conditions between Regions (CCR) depicts the encounter of regions, yielding the pressure and flow-rate equality at the interface between them.

Thereby, the following system of equations is headed for each layer:

The damaged zone (Region 1):

PDE:

$$\frac{1}{r} \frac{\partial}{\partial r} \left( r \frac{\partial p_{j1}}{\partial r} \right) = \frac{1}{\eta_{ws_j}} \frac{\partial p_{j1}}{\partial t}(r, t) \quad \text{with } r_w < r < r_{Fj} \quad \text{and } t > 0 \quad (2-4)$$

IC:

$$p_{j1}(r, t = 0) = p_j \quad (2-5)$$

For all layers, the inner boundary condition is (LEFKOVITS et al., 1961):

IBC:

$$q_{j1} = -2\pi \hat{\lambda}_{ws_j} h_j \left( r \frac{\partial p_{j1}}{\partial r} \right) \Big|_{r=r_w} \quad (2-6)$$

Region 2:

PDE:

$$\frac{1}{r} \frac{\partial}{\partial r} \left( r \frac{\partial p_{j2}}{\partial r} \right) = \frac{1}{\eta_{osj}} \frac{\partial p_{j2}}{\partial t}(r, t) \quad \text{with } r_{F_j} < r < r_{s_j} \text{ and } t > 0 \quad (2-7)$$

IC:

$$p_{j2}(r, t = 0) = p_j \quad (2-8)$$

Due to the coupling between regions 1 and 2 is known (NIE et al., 2011)

that:

CCR:

$$\begin{cases} p_{j1}(r_{F_j}, t) = p_{j2}(r_{F_j}, t) \\ q_{j1}(r_{F_j}, t) = q_{j2}(r_{F_j}, t) \end{cases} \quad (2-9)$$

Region 3:

PDE:

$$\frac{1}{r} \frac{\partial}{\partial r} \left( r \frac{\partial p_{j3}}{\partial r} \right) = \frac{1}{\eta_{orj}} \frac{\partial p_{j3}}{\partial t}(r, t) \quad \text{with } r_{s_j} < r < \infty \text{ and } t > 0 \quad (2-10)$$

IC:

$$p_{j3}(r, t = 0) = p_i \quad (2-11)$$

EBC:

$$\lim_{r \rightarrow \infty} p_{j3}(r, t) = 0 \quad (2-12)$$

Due to the coupling between regions 2 and 3, (NIE et al., 2011):

CCR:

$$\begin{cases} p_{j2}(r_{s_j}, t) = p_{j3}(r_{s_j}, t) \\ q_{j2}(r_{s_j}, t) = q_{j3}(r_{s_j}, t) \end{cases} \quad (2-13)$$

Coupling Conditions between Layers (CCL) portrays the encounter of layers by the wellbore, causing the pressure equality and due to the principle of mass conservation at the wellbore. Even though hydrostatic pressure must be considered when comparing the difference of pressure for each layer, that would be a problem for cases where the thickness is significant. Therefore in this thesis, we do not consider the hydrostatic pressure and use the equations produced (NETO et al., 2020):

CCL:

$$\begin{cases} \Delta p_{j1}(r_w, t) = \Delta p_{j+1,1}(r_w, t) \\ q_{inj} = \sum_{j=1}^n q_{j1}(r_w, t) \end{cases} \quad \text{for } j=1, \dots, (n-1) \quad (2-14)$$

Equation (2-14) does not depend on whether or not the waterfront radius has overtaken the damaged zone.

Using the Laplace transform in the equations (2-4) to (2-14) and derivations properties:

Region 1:

ODE:

$$\frac{1}{r} \frac{\partial}{\partial r} \left( r \frac{\partial \bar{p}_{j1}}{\partial r} \right) = \frac{u}{\eta_{wsj}} \bar{p}_{j1}(r, u) - \underbrace{p_{j1}(r, t=0)}_{=p_i \text{ by Eq.(2-5)}} \quad (2-15)$$

Expanding the left-hand derivative and reorganizing the terms:

$$\frac{\partial^2 \bar{p}_{j1}}{\partial \left( r \sqrt{\frac{u}{\eta_{wsj}}} \right)^2} + \frac{1}{r \sqrt{\frac{u}{\eta_{wsj}}}} \frac{\partial \bar{p}_{j1}}{\partial \left( r \sqrt{\frac{u}{\eta_{wsj}}} \right)} - \bar{p}_i = -p_i \frac{\eta_{wsj}}{u} \quad (2-16)$$

IBC:

$$\left( r \frac{\partial \bar{p}_{j1}}{\partial r} \right) \Big|_{r=r_w} = -\frac{q_{j1}}{2\pi \hat{\lambda}_{wsj} h_j} \frac{1}{u} \quad (2-17)$$

Region 2:

In the same way as region 1, the subsequent ODE is obtained:

ODE:

$$\frac{1}{r} \frac{\partial}{\partial r} \left( r \frac{\partial \bar{p}_{j2}}{\partial r} \right) = \frac{u}{\eta_{osj}} \bar{p}_{j2}(r, u) - \underbrace{p_{j2}(r, t=0)}_{=p_i \text{ by Eq.(2-8)}} \quad (2-18)$$

$$\frac{\partial^2 \bar{p}_{j2}}{\partial \left( r \sqrt{\frac{u}{\eta_{osj}}} \right)^2} + \frac{1}{r \sqrt{\frac{u}{\eta_{osj}}}} \frac{\partial \bar{p}_{j2}}{\partial \left( r \sqrt{\frac{u}{\eta_{osj}}} \right)} - \bar{p}_i = -p_i \frac{\eta_{osj}}{u} \quad (2-19)$$

Region 3:

Similarly, the following ODE is obtained:

ODE:

$$\frac{\partial^2 \bar{p}_{j3}}{\partial \left( r \sqrt{\frac{u}{\eta_{orj}}} \right)^2} + \frac{1}{r \sqrt{\frac{u}{\eta_{orj}}}} \frac{\partial \bar{p}_{j3}}{\partial \left( r \sqrt{\frac{u}{\eta_{orj}}} \right)} - \bar{p}_i = -p_i \frac{\eta_{orj}}{u} \quad (2-20)$$

EBC:

$$\lim_{r \rightarrow \infty} \bar{p}_{j3}(r, u) = \frac{p_i}{u} \quad (2-21)$$

Defining  $\Delta \bar{p}(r, u) = p_i - \bar{p}(r, u)$  and applying to the Equations (2-15) to (2-21), the following equations are obtained:

Region 1:

ODE:

$$\frac{\partial^2 \Delta \bar{p}_{j1}}{\partial \left( r \sqrt{\frac{u}{\eta_{wsj}}} \right)^2} + \frac{1}{r \sqrt{\frac{u}{\eta_{wsj}}}} \frac{\partial \Delta \bar{p}_{j1}}{\partial \left( r \sqrt{\frac{u}{\eta_{wsj}}} \right)} - \Delta \bar{p}_{j1} = 0 \quad (2-22)$$

IBC:

$$\left( r \frac{\partial \Delta \bar{p}_{j1}}{\partial r} \right) \Big|_{r=r_w} = -\frac{q_{j1}}{2\pi \hat{\lambda}_{wsj} h_j} \frac{1}{u} \quad (2-23)$$

Region 2:

ODE:

$$\frac{\partial^2 \Delta \bar{p}_{j2}}{\partial \left( r \sqrt{\frac{u}{\eta_{osj}}} \right)^2} + \frac{1}{r \sqrt{\frac{u}{\eta_{osj}}}} \frac{\partial \Delta \bar{p}_{j1}}{\partial \left( r \sqrt{\frac{u}{\eta_{osj}}} \right)} - \Delta \bar{p}_{j2} = 0 \quad (2-24)$$

For the Laplace domain, the coupling condition are given below (VIANA et al., 2022):

CCR:

$$\begin{cases} \Delta \bar{p}_{j1}(r_{F_j}, t) = \Delta \bar{p}_{j2}(r_{F_j}, t) \\ \left( r \frac{\partial \Delta \bar{p}_{j1}}{\partial r} \right) \Big|_{r=r_{F_j}} = \frac{\hat{\lambda}_{osj}}{\hat{\lambda}_{wsj}} \left( r \frac{\partial \Delta \bar{p}_{j2}}{\partial r} \right) \Big|_{r=r_{F_j}} \end{cases} \quad (\text{By Darcy's Law}) \quad (2-25)$$

Region 3:

ODE:

$$\frac{\partial^2 \Delta \bar{p}_{j3}}{\partial \left( r \sqrt{\frac{u}{\eta_{orj}}} \right)^2} + \frac{1}{r \sqrt{\frac{u}{\eta_{orj}}}} \frac{\partial \Delta \bar{p}_{j3}}{\partial \left( r \sqrt{\frac{u}{\eta_{orj}}} \right)} - \Delta \bar{p}_{j3} = 0 \quad (2-26)$$

EBC:

$$\lim_{r \rightarrow \infty} \Delta \bar{p}_{j3}(r, u) = 0 \quad (2-27)$$

CCR:

$$\begin{cases} \Delta \bar{p}_{j2}(r_{s_j}, t) = \Delta \bar{p}_{j3}(r_{s_j}, t) \\ \left( r \frac{\partial \Delta \bar{p}_{j2}}{\partial r} \right) \Big|_{r=r_{s_j}} = \frac{\hat{\lambda}_{orj}}{\hat{\lambda}_{osj}} \left( r \frac{\partial \Delta \bar{p}_{j3}}{\partial r} \right) \Big|_{r=r_{s_j}} \end{cases} \quad (\text{By Darcy's Law}) \quad (2-28)$$

CCL:

$$\begin{cases} \Delta \bar{p}_{j1}(r_w, t) = \Delta \bar{p}_{j+1,1}(r_w, t) \text{ for } j=1:(n-1) \\ q_{inj} = - \sum_{j=1}^n \left( 2\pi \hat{\lambda}_{wsj} h_j \left( r \frac{\partial \Delta \bar{p}_{j1}}{\partial r} \right) \Big|_{r=r_w} \right) \end{cases} \quad (2-29)$$

It is well-known (NETO et al., 2020) using Bessel Functions that the pressure solution in the Laplace field for any layer  $j$  and region  $i$  is:

$$\Delta \bar{p}_{ji} = A_{ji} K_0 \left( r \sqrt{\frac{u}{\eta_{flj}}} \right) + B_{ji} I_0 \left( r \sqrt{\frac{u}{\eta_{flj}}} \right) \quad (2-30)$$

where  $f = o, w$  and  $l = s, R$  depending on each reservoir part.  $A_{ji}$  and  $B_{ji}$  are coefficients to be determined. The following Bessel functions properties (ABRAMOWITZ; STEGUN, 1964) are going to be used:

$$\lim_{r \rightarrow \infty} K_0(r) = 0 \quad (2-31)$$

$$\lim_{r \rightarrow \infty} I_0(r) = \infty \quad (2-32)$$

Therefore, to satisfy Equation (2-30) and the external boundary condition of region 3, Equation (2-27),  $B_{j3}$  must be zero. Thus, the pressure solution in region 3 is:

$$\Delta\bar{p}_{j3} = A_{j3}K_0\left(r\sqrt{\frac{u}{\eta_{oR_j}}}\right) \quad (2-33)$$

By Equation (2-23) and Equation (2-29):

$$-2\pi\sum_{j=1}^n\hat{\lambda}_{ws_j}h_j\left(r\frac{\partial\Delta\bar{p}_{j1}}{\partial r}\right)\Big|_{r=r_w} = \frac{q_{inj}}{u} \quad (2-34)$$

Thus, deriving (2-30) in  $r = r_w$  and combining with equation (2-34):

$$2\pi r_w\sum_{j=1}^n\hat{\lambda}_{ws_j}h_j\sqrt{\frac{u}{\eta_{ws_j}}}\left[A_{j1}K_1\left(r_w\sqrt{\frac{u}{\eta_{ws_j}}}\right) - B_{j1}I_1\left(r_w\sqrt{\frac{u}{\eta_{ws_j}}}\right)\right] = \frac{q_{inj}}{u} \quad (2-35)$$

Combining Equation (2-25) and Equation (2-30) for  $i = 1, 2$ , that is, for region 2 and 3:

$$A_{j1}K_0\left(r_{F_j}\sqrt{\frac{u}{\eta_{ws_j}}}\right) + B_{j1}I_0\left(r_{F_j}\sqrt{\frac{u}{\eta_{ws_j}}}\right) = A_{j2}K_0\left(r_{F_j}\sqrt{\frac{u}{\eta_{os_j}}}\right) + B_{j2}I_0\left(r_{F_j}\sqrt{\frac{u}{\eta_{os_j}}}\right) \quad (2-36)$$

Moreover, deriving Equation (2-36) and using the second part of Equation (2-25):

$$\begin{aligned} & r_{F_j}\sqrt{\frac{u}{\eta_{ws_j}}}\left[-A_{j1}K_1\left(r_{F_j}\sqrt{\frac{u}{\eta_{ws_j}}}\right) + B_{j1}I_1\left(r_{F_j}\sqrt{\frac{u}{\eta_{ws_j}}}\right)\right] \\ &= \frac{\hat{\lambda}_{os_j}}{\hat{\lambda}_{ws_j}}r_{F_j}\sqrt{\frac{u}{\eta_{os_j}}}\left[-A_{j2}K_1\left(r_{F_j}\sqrt{\frac{u}{\eta_{os_j}}}\right) + B_{j2}I_1\left(r_{F_j}\sqrt{\frac{u}{\eta_{os_j}}}\right)\right] \end{aligned} \quad (2-37)$$

Thereby:

$$\begin{aligned} & A_{j1}K_1\left(r_{F_j}\sqrt{\frac{u}{\eta_{ws_j}}}\right) - B_{j1}I_1\left(r_{F_j}\sqrt{\frac{u}{\eta_{ws_j}}}\right) \\ &= \frac{\hat{\lambda}_{os_j}}{\hat{\lambda}_{ws_j}}\sqrt{\frac{\eta_{ws_j}}{\eta_{os_j}}}\left[A_{j2}K_1\left(r_{F_j}\sqrt{\frac{u}{\eta_{os_j}}}\right) - B_{j2}I_1\left(r_{F_j}\sqrt{\frac{u}{\eta_{os_j}}}\right)\right] \end{aligned} \quad (2-38)$$

Similarly, combining Equation (2-28) and Equation (2-30) for  $i = 2, 3$ :

$$A_{j2}K_0\left(r_{s_j}\sqrt{\frac{u}{\eta_{os_j}}}\right) + B_{j2}I_0\left(r_{s_j}\sqrt{\frac{u}{\eta_{os_j}}}\right) = A_{j3}K_0\left(r_{s_j}\sqrt{\frac{u}{\eta_{oR_j}}}\right) \quad (2-39)$$

In the same way, deriving Equation (2-39) and using the pressure CCR shown in Equation (2-28):

$$A_{j2}K_1\left(r_{s_j}\sqrt{\frac{u}{\eta_{os_j}}}\right) - B_{j2}I_1\left(r_{s_j}\sqrt{\frac{u}{\eta_{os_j}}}\right) = \frac{\hat{\lambda}_{oR_j}}{\hat{\lambda}_{os_j}}\sqrt{\frac{\eta_{os_j}}{\eta_{oR_j}}}A_{j3}K_1\left(r_{s_j}\sqrt{\frac{u}{\eta_{oR_j}}}\right) \quad (2-40)$$

Whereas, combining first part of Equation (2-29) and Equation (2-30):

$$\begin{aligned}
& A_{j1}K_0\left(r_w\sqrt{\frac{u}{\eta_{ws_j}}}\right) + B_{j1}I_0\left(r_w\sqrt{\frac{u}{\eta_{ws_j}}}\right) \\
& = A_{j+1,1}K_0\left(r_w\sqrt{\frac{u}{\eta_{ws_j}}}\right) + B_{j+1,1}I_0\left(r_w\sqrt{\frac{u}{\eta_{ws_j}}}\right) \text{ for } j=1,\dots,(n-1)
\end{aligned} \tag{2-41}$$

One can combine equations (2-35),(2-36), (2-38), (2-39), (2-40) in a linear system that represents the Coupling Conditions between Layers (CCL), the Coupling Conditions between Regions (CCR), the initial state (IC), and the external boundary condition (EBC), and the internal boundary condition (IBC). So it is possible to calculate the coefficients  $A_{ji}$  and  $B_{ji}$  required on Equation (2-30).

Correspondingly, considering the model where the waterfront radius exceeds the damaged zone, equations (2-35) and (2-41) will not change since they only depend on Coupling Conditions between Layers (CCL). Then, the following equations are obtained:

CCL:

$$A_{j1}K_0\left(r_{s_j}\sqrt{\frac{u}{\eta_{ws_j}}}\right) + B_{j1}I_0\left(r_{s_j}\sqrt{\frac{u}{\eta_{ws_j}}}\right) = A_{j2}K_0\left(r_{s_j}\sqrt{\frac{u}{\eta_{wR_j}}}\right) + B_{j2}I_0\left(r_{s_j}\sqrt{\frac{u}{\eta_{wR_j}}}\right) \tag{2-42}$$

CCR:

$$\begin{aligned}
& A_{j1}K_1\left(r_{s_j}\sqrt{\frac{u}{\eta_{ws_j}}}\right) - B_{j1}I_1\left(r_{s_j}\sqrt{\frac{u}{\eta_{ws_j}}}\right) \\
& = \frac{\hat{\lambda}_{wR_j}}{\hat{\lambda}_{ws_j}}\sqrt{\frac{\eta_{ws_j}}{\eta_{wR_j}}}\left[A_{j2}K_1\left(r_{s_j}\sqrt{\frac{u}{\eta_{wR_j}}}\right) - B_{j2}I_1\left(r_{s_j}\sqrt{\frac{u}{\eta_{wR_j}}}\right)\right]
\end{aligned} \tag{2-43}$$

$$A_{j2}K_0\left(r_{F_j}\sqrt{\frac{u}{\eta_{wR_j}}}\right) + B_{j2}I_0\left(r_{F_j}\sqrt{\frac{u}{\eta_{wR_j}}}\right) = A_{j3}K_0\left(r_{F_j}\sqrt{\frac{u}{\eta_{oR_j}}}\right) \tag{2-44}$$

IBC:

$$A_{j2}K_1\left(r_{F_j}\sqrt{\frac{u}{\eta_{wR_j}}}\right) - B_{j2}I_1\left(r_{F_j}\sqrt{\frac{u}{\eta_{wR_j}}}\right) = \frac{\hat{\lambda}_{oR_j}}{\hat{\lambda}_{wR_j}}\sqrt{\frac{\eta_{wR_j}}{\eta_{oR_j}}}A_{j3}K_1\left(r_{F_j}\sqrt{\frac{u}{\eta_{oR_j}}}\right) \tag{2-45}$$

For a  $n$  layer reservoir, a  $5n \times 5n$  Linear System is acquired on both methods. The matrix that represents the linear system is divided into blocks, each block representing a layer. On the model where the waterfront is within the damaged zone ( $r_F < r_s$ ), the general block attained is:

$$(M_j)_2 = \begin{array}{c} \left[ \begin{array}{cccccccc} \Delta_j K_1 \left( r_w \sqrt{\frac{u}{\eta_{ws_j}}} \right) & -\Delta_j I_1 \left( r_w \sqrt{\frac{u}{\eta_{ws_j}}} \right) & 0 & 0 & 0 & 0 & 0 & 0 \\ 0 & 0 & 0 & 0 & \dots & 0 & 0 & 0 \\ \vdots & \vdots \\ 0 & 0 & 0 & 0 & 0 & 0 & 0 & 0 \\ -K_0 \left( r_w \sqrt{\frac{u}{\eta_{ws_j}}} \right) & -I_0 \left( r_w \sqrt{\frac{u}{\eta_{ws_j}}} \right) & 0 & 0 & 0 & 0 & 0 & 0 \\ K_0 \left( r_{F_j} \sqrt{\frac{u}{\eta_{os_j}}} \right) & I_0 \left( r_{F_j} \sqrt{\frac{u}{\eta_{os_j}}} \right) & -K_0 \left( r_{F_j} \sqrt{\frac{u}{\eta_{os_j}}} \right) & -I_0 \left( r_{F_j} \sqrt{\frac{u}{\eta_{os_j}}} \right) & 0 & 0 & 0 & 0 \\ K_1 \left( r_{F_j} \sqrt{\frac{u}{\eta_{os_j}}} \right) & -I_1 \left( r_{F_j} \sqrt{\frac{u}{\eta_{os_j}}} \right) & -\Gamma_{j_2} K_1 \left( r_{F_j} \sqrt{\frac{u}{\eta_{os_j}}} \right) & \Gamma_{j_2} I_1 \left( r_{F_j} \sqrt{\frac{u}{\eta_{os_j}}} \right) & 0 & 0 & 0 & 0 \\ 0 & 0 & 0 & 0 & 0 & 0 & 0 & 0 \\ 0 & 0 & 0 & 0 & 0 & 0 & 0 & 0 \\ K_0 \left( r_w \sqrt{\frac{u}{\eta_{ws_j}}} \right) & I_0 \left( r_w \sqrt{\frac{u}{\eta_{ws_j}}} \right) & 0 & 0 & 0 & 0 & 0 & 0 \\ 0 & 0 & 0 & 0 & \dots & 0 & 0 & 0 \\ 0 & 0 & 0 & 0 & 0 & 0 & 0 & 0 \end{array} \right] \begin{array}{c} \leftarrow 5(j-1) - 1 \rightarrow \\ \\ \\ \\ \\ \\ \\ \\ \\ \\ \\ \leftarrow 5(n-j) - 1 \rightarrow \end{array} \end{array} \quad (2-46)$$

Equation (2-46) only works for  $j = 2, \dots, (n-1)$ , that is, for all layers except the first and last. The constants  $\Delta_j$ ,  $\Gamma_{j_2}$  and  $\Lambda_{j_2}$  are defined as follows:

$$\Delta_j = 2\pi r_w \hat{\lambda}_{ws_j} h_j \sqrt{\frac{u}{\eta_{ws_j}}}, \Gamma_{j_2} = \frac{\hat{\lambda}_{os_j}}{\hat{\lambda}_{ws_j}}, \sqrt{\frac{\eta_{ws_j}}{\eta_{os_j}}}, \Lambda_{j_2} = \frac{\hat{\lambda}_{oR_j}}{\hat{\lambda}_{os_j}} \sqrt{\frac{\eta_{os_j}}{\eta_{oR_j}}} \quad (2-47)$$

For  $j = 1$  and  $j = n$ , the matrix blocks are:

$$(M_1)_2 = \begin{bmatrix}
 \Delta_1 K_1 \left( r_w \sqrt{\frac{u}{\eta_{ws1}}} \right) & -\Delta_1 I_1 \left( r_w \sqrt{\frac{u}{\eta_{ws1}}} \right) & 0 & 0 & 0 \\
 K_0 \left( r_{F1} \sqrt{\frac{u}{\eta_{ws1}}} \right) & I_0 \left( r_{F1} \sqrt{\frac{u}{\eta_{ws1}}} \right) & -K_0 \left( r_{F1} \sqrt{\frac{u}{\eta_{os1}}} \right) & -I_0 \left( r_{F1} \sqrt{\frac{u}{\eta_{os1}}} \right) & 0 \\
 K_1 \left( r_{F1} \sqrt{\frac{u}{\eta_{ws1}}} \right) & -I_1 \left( r_{F1} \sqrt{\frac{u}{\eta_{ws1}}} \right) & -\Gamma_{12} K_1 \left( r_{F1} \sqrt{\frac{u}{\eta_{os1}}} \right) & \Gamma_{12} I_1 \left( r_{F1} \sqrt{\frac{u}{\eta_{os1}}} \right) & 0 \\
 0 & 0 & K_0 \left( r_{s1} \sqrt{\frac{u}{\eta_{os1}}} \right) & I_0 \left( r_{s1} \sqrt{\frac{u}{\eta_{os1}}} \right) & -K_0 \left( r_{s1} \sqrt{\frac{u}{\eta_{oR1}}} \right) \\
 0 & 0 & K_1 \left( r_{s1} \sqrt{\frac{u}{\eta_{os1}}} \right) & -I_1 \left( r_{s1} \sqrt{\frac{u}{\eta_{os1}}} \right) & -\Lambda_{12} K_1 \left( r_{s1} \sqrt{\frac{u}{\eta_{oR1}}} \right) \\
 K_0 \left( r_w \sqrt{\frac{u}{\eta_{ws1}}} \right) & I_0 \left( r_w \sqrt{\frac{u}{\eta_{ws1}}} \right) & 0 & 0 & 0 \\
 0 & 0 & 0 & 0 & 0 \\
 \vdots & \vdots & \vdots & \vdots & \vdots \\
 0 & 0 & 0 & 0 & 0
 \end{bmatrix} \begin{matrix} \\ \\ \\ \\ \\ \\ \\ \\ \\ \leftarrow 5(n-1) - 1 \rightarrow\end{matrix}$$

(2-48)

$$(M_n)_2 = \begin{array}{c} \left[ \begin{array}{cccccccc} \Delta_n K_1 \left( r_w \sqrt{\frac{u}{\eta_{ws_n}}} \right) & -\Delta_n I_1 \left( r_w \sqrt{\frac{u}{\eta_{ws_n}}} \right) & 0 & 0 & 0 & 0 & 0 & 0 \\ 0 & 0 & 0 & 0 & 0 & 0 & 0 & 0 \\ \vdots & \vdots \\ 0 & 0 & 0 & 0 & 0 & 0 & 0 & 0 \\ -K_0 \left( r_w \sqrt{\frac{u}{\eta_{ws_n}}} \right) & -I_0 \left( r_w \sqrt{\frac{u}{\eta_{ws_n}}} \right) & 0 & 0 & 0 & 0 & 0 & 0 \\ K_0 \left( r_{F_n} \sqrt{\frac{u}{\eta_{os_n}}} \right) & I_0 \left( r_{F_n} \sqrt{\frac{u}{\eta_{os_n}}} \right) & -K_0 \left( r_{F_n} \sqrt{\frac{u}{\eta_{os_n}}} \right) & -I_0 \left( r_{F_n} \sqrt{\frac{u}{\eta_{os_n}}} \right) & 0 & 0 & 0 & 0 \\ K_1 \left( r_{F_n} \sqrt{\frac{u}{\eta_{ws_n}}} \right) & -I_1 \left( r_{F_n} \sqrt{\frac{u}{\eta_{ws_n}}} \right) & -\Gamma_{n_2} K_1 \left( r_{F_n} \sqrt{\frac{u}{\eta_{os_n}}} \right) & \Gamma_{n_2} I_1 \left( r_{F_n} \sqrt{\frac{u}{\eta_{os_n}}} \right) & 0 & 0 & 0 & 0 \\ 0 & 0 & K_0 \left( r_{s_n} \sqrt{\frac{u}{\eta_{os_n}}} \right) & I_0 \left( r_{s_n} \sqrt{\frac{u}{\eta_{os_n}}} \right) & -K_0 \left( r_{s_n} \sqrt{\frac{u}{\eta_{os_n}}} \right) & -\Lambda_{n_2} K_1 \left( r_{s_n} \sqrt{\frac{u}{\eta_{os_n}}} \right) & 0 & 0 \\ 0 & 0 & K_1 \left( r_{s_n} \sqrt{\frac{u}{\eta_{os_n}}} \right) & -I_1 \left( r_{s_n} \sqrt{\frac{u}{\eta_{os_n}}} \right) & -I_1 \left( r_{s_n} \sqrt{\frac{u}{\eta_{os_n}}} \right) & -\Lambda_{n_2} K_1 \left( r_{s_n} \sqrt{\frac{u}{\eta_{os_n}}} \right) & 0 & 0 \end{array} \right] \\ \leftarrow 5(n-1) - 1 \rightarrow \end{array} \quad (2-49)$$

If  $n = 1$ , only the first six lines of the matrix presented in Equation (2-48) are considered.

Similarly, for the first model (considering  $r_F > r_s$ ), the general block and blocks for  $j = 1$  and  $j = n$  are:

$$\begin{aligned}
 (M_j)_1 = & \left[ \begin{array}{cccccccc}
 \Delta_j K_1 \left( r_w \sqrt{\frac{u}{\eta_{ws_j}}} \right) & -\Delta_j I_1 \left( r_w \sqrt{\frac{u}{\eta_{ws_j}}} \right) & 0 & 0 & 0 & 0 & 0 & 0 \\
 0 & 0 & 0 & 0 & \vdots & 0 & 0 & 0 \\
 \vdots & \vdots & \vdots & \vdots & 0 & \vdots & \vdots & \vdots \\
 0 & 0 & 0 & 0 & 0 & 0 & 0 & 0 \\
 -K_0 \left( r_w \sqrt{\frac{u}{\eta_{ws_j}}} \right) & -I_0 \left( r_w \sqrt{\frac{u}{\eta_{ws_j}}} \right) & -I_0 \left( r_{s_j} \sqrt{\frac{u}{\eta_{ws_j}}} \right) & -K_0 \left( r_{s_j} \sqrt{\frac{u}{\eta_{ws_j}}} \right) & -I_0 \left( r_{s_j} \sqrt{\frac{u}{\eta_{ws_j}}} \right) & -I_0 \left( r_{s_j} \sqrt{\frac{u}{\eta_{ws_j}}} \right) & -I_0 \left( r_{s_j} \sqrt{\frac{u}{\eta_{ws_j}}} \right) & 0 \\
 K_0 \left( r_{s_j} \sqrt{\frac{u}{\eta_{ws_j}}} \right) & I_0 \left( r_{s_j} \sqrt{\frac{u}{\eta_{ws_j}}} \right) & I_0 \left( r_{s_j} \sqrt{\frac{u}{\eta_{ws_j}}} \right) & -\Gamma_{j_1} K_1 \left( r_{s_j} \sqrt{\frac{u}{\eta_{ws_j}}} \right) & -I_0 \left( r_{s_j} \sqrt{\frac{u}{\eta_{ws_j}}} \right) & -I_0 \left( r_{s_j} \sqrt{\frac{u}{\eta_{ws_j}}} \right) & -I_0 \left( r_{s_j} \sqrt{\frac{u}{\eta_{ws_j}}} \right) & 0 \\
 K_1 \left( r_{s_j} \sqrt{\frac{u}{\eta_{ws_j}}} \right) & -I_1 \left( r_{s_j} \sqrt{\frac{u}{\eta_{ws_j}}} \right) & -I_1 \left( r_{s_j} \sqrt{\frac{u}{\eta_{ws_j}}} \right) & -\Gamma_{j_1} K_1 \left( r_{s_j} \sqrt{\frac{u}{\eta_{ws_j}}} \right) & -I_1 \left( r_{s_j} \sqrt{\frac{u}{\eta_{ws_j}}} \right) & -I_1 \left( r_{s_j} \sqrt{\frac{u}{\eta_{ws_j}}} \right) & -I_1 \left( r_{s_j} \sqrt{\frac{u}{\eta_{ws_j}}} \right) & 0 \\
 0 & 0 & 0 & K_0 \left( r_{F_j} \sqrt{\frac{u}{\eta_{wR_j}}} \right) & I_0 \left( r_{F_j} \sqrt{\frac{u}{\eta_{wR_j}}} \right) & I_0 \left( r_{F_j} \sqrt{\frac{u}{\eta_{wR_j}}} \right) & I_0 \left( r_{F_j} \sqrt{\frac{u}{\eta_{wR_j}}} \right) & -K_0 \left( r_{F_j} \sqrt{\frac{u}{\eta_{wR_j}}} \right) \\
 0 & 0 & 0 & K_1 \left( r_{F_j} \sqrt{\frac{u}{\eta_{wR_j}}} \right) & -I_1 \left( r_{F_j} \sqrt{\frac{u}{\eta_{wR_j}}} \right) & -I_1 \left( r_{F_j} \sqrt{\frac{u}{\eta_{wR_j}}} \right) & -I_1 \left( r_{F_j} \sqrt{\frac{u}{\eta_{wR_j}}} \right) & -\Lambda_{j_1} K_1 \left( r_{F_j} \sqrt{\frac{u}{\eta_{wR_j}}} \right) \\
 K_0 \left( r_w \sqrt{\frac{u}{\eta_{ws_j}}} \right) & I_0 \left( r_w \sqrt{\frac{u}{\eta_{ws_j}}} \right) & 0 & 0 & 0 & 0 & 0 & 0 \\
 0 & 0 & 0 & 0 & 0 & 0 & 0 & 0 \\
 \vdots & \vdots \\
 0 & 0 & 0 & 0 & 0 & 0 & 0 & 0
 \end{array} \right]
 \end{aligned}
 \tag{2-50}$$

The constants  $\Gamma_{j_1}$  and  $\Lambda_{j_1}$  are defined as below:

$$\Gamma_{j_1} = \frac{\hat{\lambda}_{wR_j}}{\hat{\lambda}_{ws_j}}, \sqrt{\frac{\eta_{ws_j}}{\eta_{wR_j}}}, \Lambda_{j_1} = \frac{\hat{\lambda}_{oR_j}}{\hat{\lambda}_{wR_j}} \sqrt{\frac{\eta_{wR_j}}{\eta_{oR_j}}}
 \tag{2-51}$$

$$(M_1)_1 = \left[ \begin{array}{cccccccc}
 \Delta_1 K_1 \left( r_w \sqrt{\frac{u}{\eta_{ws1}}} \right) & -\Delta_1 I_1 \left( r_w \sqrt{\frac{u}{\eta_{ws1}}} \right) & 0 & 0 & 0 & 0 & 0 & 0 \\
 K_0 \left( r_{s1} \sqrt{\frac{u}{\eta_{ws1}}} \right) & I_0 \left( r_{s1} \sqrt{\frac{u}{\eta_{ws1}}} \right) & -K_0 \left( r_{s1} \sqrt{\frac{u}{\eta_{wR_1}}} \right) & -I_0 \left( r_{s1} \sqrt{\frac{u}{\eta_{wR_1}}} \right) & 0 & 0 & 0 & 0 \\
 K_1 \left( r_{s1} \sqrt{\frac{u}{\eta_{ws1}}} \right) & -I_1 \left( r_{s1} \sqrt{\frac{u}{\eta_{ws1}}} \right) & -\Gamma_{12} K_1 \left( r_{s1} \sqrt{\frac{u}{\eta_{wR_1}}} \right) & \Gamma_{12} I_1 \left( r_{s1} \sqrt{\frac{u}{\eta_{wR_1}}} \right) & 0 & 0 & 0 & 0 \\
 0 & 0 & K_0 \left( r_{F_1} \sqrt{\frac{u}{\eta_{wR_1}}} \right) & I_0 \left( r_{F_1} \sqrt{\frac{u}{\eta_{wR_1}}} \right) & -K_0 \left( r_{F_1} \sqrt{\frac{u}{\eta_{oR_1}}} \right) & 0 & 0 & 0 \\
 K_0 \left( r_w \sqrt{\frac{u}{\eta_{ws1}}} \right) & I_0 \left( r_w \sqrt{\frac{u}{\eta_{ws1}}} \right) & K_1 \left( r_{F_1} \sqrt{\frac{u}{\eta_{wR_1}}} \right) & -I_1 \left( r_{F_1} \sqrt{\frac{u}{\eta_{wR_1}}} \right) & -\Lambda_{12} K_1 \left( r_{F_1} \sqrt{\frac{u}{\eta_{oR_1}}} \right) & 0 & 0 & 0 \\
 0 & 0 & 0 & 0 & 0 & 0 & 0 & 0 \\
 \vdots & \vdots \\
 0 & 0 & 0 & 0 & 0 & 0 & 0 & 0
 \end{array} \right] \quad \leftarrow 5(n-1) - 1 \rightarrow$$

(2-52)

$$(M_n)_1 = \begin{array}{c} \left[ \begin{array}{cccccccc} \Delta_n K_1 \left( r_w \sqrt{\frac{u}{\eta_{ws_n}}} \right) & -\Delta_n I_1 \left( r_w \sqrt{\frac{u}{\eta_{ws_n}}} \right) & 0 & 0 & 0 & 0 & 0 & 0 \\ 0 & 0 & 0 & 0 & \dots & 0 & 0 & 0 \\ \vdots & \vdots \\ 0 & 0 & 0 & 0 & 0 & 0 & 0 & 0 \\ -K_0 \left( r_w \sqrt{\frac{u}{\eta_{ws_n}}} \right) & -I_0 \left( r_w \sqrt{\frac{u}{\eta_{ws_n}}} \right) & 0 & 0 & 0 & 0 & 0 & 0 \\ K_0 \left( r_{s_n} \sqrt{\frac{u}{\eta_{ws_n}}} \right) & I_0 \left( r_{s_n} \sqrt{\frac{u}{\eta_{ws_n}}} \right) & -K_0 \left( r_{s_n} \sqrt{\frac{u}{\eta_{ws_n}}} \right) & -I_0 \left( r_{s_n} \sqrt{\frac{u}{\eta_{ws_n}}} \right) & 0 & 0 & 0 & 0 \\ K_1 \left( r_{s_n} \sqrt{\frac{u}{\eta_{ws_n}}} \right) & -I_1 \left( r_{s_n} \sqrt{\frac{u}{\eta_{ws_n}}} \right) & -\Gamma_{n_2} K_1 \left( r_{s_n} \sqrt{\frac{u}{\eta_{ws_n}}} \right) & \Gamma_{n_2} I_1 \left( r_{s_n} \sqrt{\frac{u}{\eta_{ws_n}}} \right) & 0 & 0 & 0 & 0 \\ 0 & 0 & K_0 \left( r_{F_n} \sqrt{\frac{u}{\eta_{ws_n}}} \right) & I_0 \left( r_{F_n} \sqrt{\frac{u}{\eta_{ws_n}}} \right) & -K_0 \left( r_{F_n} \sqrt{\frac{u}{\eta_{ws_n}}} \right) & -I_0 \left( r_{F_n} \sqrt{\frac{u}{\eta_{ws_n}}} \right) & 0 & 0 \\ 0 & 0 & K_1 \left( r_{F_n} \sqrt{\frac{u}{\eta_{ws_n}}} \right) & -I_1 \left( r_{F_n} \sqrt{\frac{u}{\eta_{ws_n}}} \right) & -\Lambda_{n_2} K_1 \left( r_{F_n} \sqrt{\frac{u}{\eta_{ws_n}}} \right) & \Lambda_{n_2} I_1 \left( r_{F_n} \sqrt{\frac{u}{\eta_{ws_n}}} \right) & -K_0 \left( r_{F_n} \sqrt{\frac{u}{\eta_{ws_n}}} \right) & -I_0 \left( r_{F_n} \sqrt{\frac{u}{\eta_{ws_n}}} \right) \end{array} \right] \\ \leftarrow 5(n-1)-1 \rightarrow \end{array} \quad (2-53)$$

Regardless of the model, the subsequent modifications are applied if there is no skin zone on the  $j$ th layer:

$$\begin{aligned}
\eta_{ws_j} &= \eta_w R_j \\
\lambda_{ws_j} &= \lambda_w R_j \\
\eta_{os_j} &= \eta_o R_j \\
\lambda_{os_j} &= \lambda_o R_j;
\end{aligned} \quad (2-54)$$

Thereby, the  $5n \times 5n$  Linear System may be expressed as:

$$M \begin{bmatrix} A_{11} \\ B_{11} \\ A_{12} \\ B_{12} \\ A_{13} \\ \vdots \\ A_{n1} \\ B_{n1} \\ A_{n2} \\ B_{n2} \\ A_{n3} \end{bmatrix} = \begin{bmatrix} q_{inj} \\ u \\ 0 \\ \vdots \\ 0 \end{bmatrix} \quad (2-55)$$

Using an index  $m$  representing the model, the matrix  $M$  is defined as below:

$$M = [(M_1)_m \quad (M_2)_m \quad \dots \quad (M_n)_m] \quad (2-56)$$

Therefore, once the coefficients  $A_{11}$  and  $B_{11}$  are determined, in the Laplace domain, the well pressure solution is given (NETO et al., 2020) by:

$$\Delta \bar{p}_{wf} = A_{11} K_0 \left( r_w \sqrt{\frac{u}{\eta_{ws1}}} \right) + B_{11} I_0 \left( r_w \sqrt{\frac{u}{\eta_{ws1}}} \right) \quad (2-57)$$

Furthermore, Equation (2-6) correlates the pressure difference derivative and the sandface flow-rate at each layer. In the Laplace field is possible to obtain:

$$\bar{q}_{j1} = -2\pi u \hat{\lambda}_{wsj} h_j \left( r \frac{\partial \Delta \bar{p}_{j1}}{\partial r} \right) \Big|_{r=r_w} \quad (2-58)$$

The pressure difference profile presented in Equation (2-57) and the flow-rate response given in Equation (2-58) can be converted to the real domain through Stehfest Algorithm (STEHFEST, 1970).

## 3

### Ensemble-Based Methods

Ensemble-Based Methods have been widely applied to data assimilation as an alternative to gradient-based algorithms (SILVA et al., 2021). One of the biggest hurdles is the gradient calculation, which may not be simple and computationally demanding. These Ensemble-Based Methods have the advantage of not calculating the gradient vector but using statistics for estimating derivatives.

Among the ensemble-based methods, the Ensemble Smoother (LEEuwEN; EVENSEN, 1996) became a viable alternative in situations where the restart required by the Ensemble Kalman Filter (EVENSEN, 1994) was an obstacle. Nonetheless, Ensemble Smoother uses only one assimilation step, making data estimation less efficient. A viable alternative is the Ensemble Smoother with Multiple Data Assimilation (EMERICK; REYNOLDS, 2013).

#### 3.1

##### Bayesian Statistics

Bayesian statistics are used to estimate the uncertainty related to our data. This mechanism is advantageous for inverse problems due to the significant lack of data and the high number of parameters to be estimated. Besides, there are also errors yielded in the data measurement, which makes an estimation of our data-related uncertainty desirable (SILVA; PESCO; JR, 2021).

This thesis presents a data-matching problem in reservoir engineering. The data's inaccuracy is relevant since it is intrinsically an inverse problem, subject to reflect on when estimating model parameters such that their production simulated responses match the observed data. As reservoir models are often rough approximations of the actual models, a probabilistic view considers the uncertainty related to the model and the data (SILVA; PESCO; JR, 2021).

##### 3.1.1

###### Linear Problem

Consider  $m \in \mathbb{R}^{N_m}$  a vector of parameters and a data vector  $d \in \mathbb{R}^{N_d}$  with  $N_m$  being the number of parameters used and  $N_d$  the number of data. The relation between these two vectors is:

$$d = Gm \tag{3-1}$$

where  $G \in \mathbb{R}^{N_d \times N_m}$  is the sensitivity matrix of the data. If  $d$  is the observed data  $d_{obs}$ , equation (3-1) must be adapted due to the measurement error. Assuming there is no error in the model parameters:

$$d_{obs} = Gm + \epsilon \quad (3-2)$$

where  $\epsilon \in \mathbb{R}^{N_d}$ . In this thesis, this error is considered to be Gaussian with zero mean and covariance  $C_d \in \mathbb{R}^{N_d \times N_d}$ . Thus, one can write down its probability density function (PDF) as:

$$f(\epsilon) = c_1 \times \exp\left\{-\frac{1}{2}(d_{obs} - Gm)^T C_d^{-1}(d_{obs} - Gm)\right\} \quad (3-3)$$

Where  $c_1$  is a normalizing constant.

Suppose our vector of model parameters parameter  $m$  is initially uncertain. Considering that  $m$  also assumes Gaussian distribution, one can write down its prior PDF as:

$$f(m) = c_2 \times \exp\left\{-\frac{1}{2}(m - m_{pr})^T C_m^{-1}(m - m_{pr})\right\} \quad (3-4)$$

Where  $c_2$  is a constant and  $m_{pr}$  is the prior estimate of the variables and  $C_m$  is the prior covariance of the model variable.

Using Bayes' rule, it is possible to estimate the probability density function of the model parameters given our observed data:

$$f(m|d_{obs}) = \frac{f(d_{obs}|m)f(m)}{f(d_{obs})} \quad (3-5)$$

Due to equation (3-2), the probability of measuring  $d_{obs}$  given the vector of model parameters  $m$  is the probability of the error  $\epsilon$ :

$$f(d_{obs}|m) = f(\epsilon) \quad (3-6)$$

Using Equations (3-3) to (3-6):

$$f(m|d_{obs}) = c_3 \times \exp\left\{-\frac{1}{2}(d_{obs} - Gm)^T C_d^{-1}(d_{obs} - Gm) - \frac{1}{2}(m - m_{pr})^T C_m^{-1}(m - m_{pr})\right\} \quad (3-7)$$

where  $c_3$  is a constant. Commonly the following notation is used:

$$f(m|d_{obs}) = a \times \exp\{-O(m)\} \quad (3-8)$$

where  $a$  is a normalizing constant and  $O(m)$  is the objective function, defined as:

$$O(m) = \frac{1}{2}(d_{obs} - Gm)^T C_d^{-1}(d_{obs} - Gm) + \frac{1}{2}(m - m_{pr})^T C_m^{-1}(m - m_{pr}) \quad (3-9)$$

In order to maximize  $f(m|d_{obs})$ , the minimization of the Objective

Function  $O(m)$  is aimed.

### 3.1.2

#### Maximum a posteriori estimate

Since the relation between parameters is linear, the objective function  $O(m)$  is quadratic for any model parameter  $m \in \mathbb{R}^{N_m}$ . With the intention of minimizing  $O(m)$ , the gradient  $\nabla O(m)$  and its associated Hessian matrix  $\nabla^2 O(m)$  are calculated as:

$$\nabla O(m) = G^T C_d^{-1}(Gm - d_{obs}) + C_m^{-1}(m - m_{pr}) \quad (3-10)$$

$$\nabla^2 O(m) = G^T C_d^{-1} G + C_m^{-1} \quad (3-11)$$

Focusing on equation (3-11) and knowing that  $C_d^{-1}$  and  $C_m^{-1}$  are symmetric:

$$\begin{aligned} (\nabla^2 O(m))^T &= (G^T C_d^{-1} G + C_m^{-1})^T \\ &= (G^T C_d^{-1} G)^T + (C_m^{-1})^T \\ &= (G^T (C_d^{-1})^T G) + (C_m^{-1})^T \\ &= G^T C_d^{-1} G + C_m^{-1} \end{aligned} \quad (3-12)$$

Therefore,  $\nabla^2 O(m)$  is symmetric. Likewise, assuming that both  $C_d^{-1}$  and  $C_m^{-1}$  are positive-definite, given a non-null arbitrary vector  $x \in \mathbb{R}^m$ :

$$\begin{aligned} x^T \nabla^2 O(m) x &= x^T (G^T C_d^{-1} G + C_m^{-1}) x \\ &= x^T G^T C_d^{-1} G x + x^T C_m^{-1} x \\ &= (Gx)^T C_d^{-1} G x + x^T C_m^{-1} x > 0 \end{aligned} \quad (3-13)$$

Hence,  $\nabla^2 O(m)$  is also positive-definite. Thereby,  $O(m)$  has an unique minimum, obtained by setting  $\nabla O(m)$  as zero:

$$\begin{aligned} \nabla O(m) &= 0 \\ G^T C_d^{-1}(Gm - d_{obs}) + C_m^{-1}(m - m_{pr}) &= 0 \\ G^T C_d^{-1}(Gm - Gm_{pr} + Gm_{pr} - d_{obs}) + C_m^{-1}(m - m_{pr}) &= 0 \\ G^T C_d^{-1}(Gm - Gm_{pr}) + G^T C_d^{-1}(Gm_{pr} - d_{obs}) + C_m^{-1}(m - m_{pr}) &= 0 \\ G^T C_d^{-1}G(m - m_{pr}) + G^T C_d^{-1}(Gm_{pr} - d_{obs}) + C_m^{-1}(m - m_{pr}) &= 0 \\ (C_m^{-1} + G^T C_d^{-1}G)(m - m_{pr}) + G^T C_d^{-1}(Gm_{pr} - d_{obs}) &= 0 \end{aligned} \quad (3-14)$$

From Equation (3-14), it is possible to determine the value of  $m$  such that the minimum of  $O(m)$  is obtained and, therefore the maximum of  $f(m|d_{obs})$ . This vector is the maximum a posteriori estimate to the vector of model parameters, denoted by  $m_{map}$ .

$$m_{map} = m_{pr} + (C_m^{-1} + G^T C_d^{-1} G)^{-1} G^T C_d^{-1} (d_{obs} - Gm_{pr}) \quad (3-15)$$

### 3.2

#### Ensemble Smoother

The Ensemble Smoother is an ensemble-based method that approximates our sensitivity matrix using ensembles to estimate our vector of model parameters. Since there is no need to calculate the gradient vector, there is an advantage in its computational use of it. This section will discuss the equations used in the Ensemble Smoother, the iterative way to improve it (Ensemble Smoother With Multiple Data Assimilation (EMERICK; REYNOLDS, 2013)), and finally, a way to use it iteratively without problems with dimension differences in the data.

Considering the relation between the data  $d \in \mathbb{R}^{N_d}$  and vector of model parameters  $m \in \mathbb{R}^{N_m}$  to be linear (Equation (3-1)), with the sensitivity matrix  $G \in \mathbb{R}^{N_d \times N_m}$ , an ensemble of model parameters vector  $\{m\}_j$  is created, where  $j = 1 \dots N_e$  and  $N_e \in \mathbb{N}$  is the ensemble size. Thereby, an ensemble of the data  $\{d\}_j$  is also produced, with  $d_j = Gm_j$ . It is possible to estimate the covariance matrix of the model parameters  $C_m$ :

$$C_m \approx \frac{1}{N_e - 1} \sum_{j=1}^{N_e} (m_j - \bar{m})(m_j - \bar{m})^T \quad (3-16)$$

where  $\bar{m}$  is the mean of the ensemble of model parameters vectors. Using equation (3-16), it is possible to approximate the matrices  $C_m G^T$  and  $G C_m G^T$  presented in the equation (3-15) that defines the maximum a posteriori estimate to the vector of model parameters.

$$\begin{aligned} C_m G^T &\approx \left( \frac{1}{N_e - 1} \sum_{j=1}^{N_e} (m_j - \bar{m})(m_j - \bar{m})^T \right) G^T \\ &\approx \frac{1}{N_e - 1} \sum_{j=1}^{N_e} (m_j - \bar{m})(m_j - \bar{m})^T G^T \\ &\approx \frac{1}{N_e - 1} \sum_{j=1}^{N_e} (m_j - \bar{m})(G(m_j - \bar{m}))^T \end{aligned} \quad (3-17)$$

Using Equation (3-17) and assuming  $\bar{d} = G\bar{m}$ , the following approximation is obtained:

$$\begin{aligned} C_m G^T &\approx \frac{1}{N_e - 1} \sum_{j=1}^{N_e} (m_j - \bar{m})(d_j - \bar{d})^T \\ &\approx C_{md} \end{aligned} \quad (3-18)$$

where  $C_{md}$  is the cross-covariance matrix between the vector of model parameters  $m$  and the data vector  $d$ . Likewise, it is possible to approximate the matrix

$GC_m G^T$ , using equation (3-18):

$$\begin{aligned}
 GC_m G^T &\approx G \left( \frac{1}{N_e - 1} \sum_{j=1}^{N_e} (m_j - \bar{m})(d_j - \bar{d})^T \right) \\
 &\approx \frac{1}{N_e - 1} \sum_{j=1}^{N_e} G(m_j - \bar{m})(d_j - \bar{d})^T \\
 &\approx \frac{1}{N_e - 1} \sum_{j=1}^{N_e} (d_j - \bar{d})(d_j - \bar{d})^T \\
 &\approx C_{dd}
 \end{aligned} \tag{3-19}$$

where  $C_{dd}$  is the auto-covariance matrix of the data  $d$ . It is possible to update Equation (3-15) using the approximations given by Equations (3-18), (3-19) and the following identity:

$$(C_m^{-1} + G^T C_d^{-1} G)^{-1} G^T C_d^{-1} = C_m G^T (GC_m G^T + C_d)^{-1} \tag{3-20}$$

Therefore, one may compute  $m_{map}$  as:

$$m_{map} = m_{pr} + C_{md}(C_{dd} + C_d)^{-1}(d_{obs} - Gm_{pr}) \tag{3-21}$$

The Ensemble Smoother updates each ensemble member's model of parameters  $m$ . Therefore the analyzed vector of model parameters is defined for  $j = 1..N_e$  as:

$$m_j^a = m_j^f + C_{md}^f(C_{dd} + C_d)^{-1}(d_{uc,j} - d_j^f) \tag{3-22}$$

Here,  $a$  depicts the analysis step, and  $f$  refers to the forward step. The vector  $d_{uc,j}$  is the perturbed observed data,  $d_{uc,j} \sim \mathcal{N}(d_{obs}, C_d)$ .

Nevertheless, the Ensemble Smoother is not expected to produce trustable estimates of the vector of model parameters in nonlinear problems, such as most history-matching problems. Mainly since (REYNOLDS; ZAFARI; LI, 2006) has shown that the Ensemble Smoother update process is alike to applying a single Gauss-Newton iteration with full-step size using the sensitivity matrix estimated from the prior ensemble. To avoid this hurdle, iterated forms of Ensemble Smoother were proposed, such as the Ensemble Smoother with Multiple Data Assimilation (ES-MDA), which assimilates the same data multiple times.

### 3.2.1

#### Ensemble Smoother with Multiple Data Assimilation

Using the ensemble smoother, we apply a single Gauss-Newton correction and considering a Multiple Data Assimilation, it is possible to develop, in a

sense, an iterative ensemble smoother. Thereby, more mine corrections in the ensemble are executed. The covariance matrix associated is inflated, aiming to absorb the changes in the model. The updated equation of the vector of model parameters is defined as:

$$m_j^{k+1} = m_j^k + C_{md}^k (C_{dd}^k + \alpha_{k+1} C_d)^{-1} (d_{uc,j}^k - d_j^k) \quad (3-23)$$

where  $k = 0, \dots, N_a - 1$  and  $N_a \geq 1$  is the number of assimilations, and  $j = 1, \dots, N_e$ . The set  $\{\alpha_i\}_{i=1}^{N_a}$  refers to the set of the inflation factors, which must satisfy the following equation:

$$\sum_{i=1}^{N_a} \frac{1}{\alpha_i} = 1 \quad (3-24)$$

The proof of Equation (3-24) is shown in (EMERICK; REYNOLDS, 2013) and the exigency of Equation (3-24) is due to the necessity to establish the equivalence between the single and multiple data assimilation, i.e., the vector of model parameters obtained in Equation (3-22) has to be a sample of the posterior probability density function. An important consequence of Equation (3-24) is that  $\alpha_k \geq 1, \forall k$ , aiding the choice of these inflation factors.

The covariance matrices approximated from the ensemble can also be defined as:

$$C_{md}^k = \Delta M^k (\Delta D^k)^T \quad (3-25)$$

$$C_{dd}^k = \Delta D^k (\Delta D^k)^T \quad (3-26)$$

Where:

$$\Delta M^k = \frac{1}{\sqrt{N_e - 1}} (m^k - \bar{m}^k) \quad (3-27)$$

$$\Delta D^k = \frac{1}{\sqrt{N_e - 1}} (d^k - \bar{d}^k) \quad (3-28)$$

Thereby, the ES-MDA algorithm is summarized as follows:

1. Choose the number of assimilations  $N_a \geq 1$ , the number of ensembles  $N_e \geq 1$  and the inflation factors  $\alpha_k$ .
2. For  $i = 1, \dots, N_a$ :
  - (a) Run the ensemble from time zero.
  - (b) For  $j = 1, \dots, N_e$ :
    - i. Perturb the observation vector using  $d_{uc,j} = d_{obs} + \sqrt{\alpha_i} C_d^{1/2} z_{d,j}$ , with  $z_{d,j} \sim \mathcal{N}(0, I_{N_d})$ .
  - (c) Update the ensemble using Equation (3-22).

Note that, for each assimilation,  $d_{uc}$  is recomputed. The mentioned procedure reduces the problem of matching outliers in the ensemble (EMERICK;

REYNOLDS, 2013). Nonetheless, by using a MDA process, the values of  $N_a$  and all inflation factors  $\{\alpha_k\}_{k=1}^{N_a}$  must be selected before the data assimilation.

One simple choice for all  $\alpha_k$  is  $\alpha_k = N_a, \forall k$ . Note that this alternative regards Equation (3-24). Despite this, other options were built, such as (LE; EMERICK; REYNOLDS, 2016) and (RAFIEE; REYNOLDS, 2017), assuming decreasing values of  $\alpha_k$  and invariably using the Equation (3-24).

Regarding the number of assimilations  $N_a$  and also the number of ensembles  $N_e$ , that must be appropriate, primarily owing to the relation between these numbers and the computational cost, (SILVA et al., 2021) indicated a suitable set of values for these numbers in the ES-MDA considering a specific problem of estimating individual layer properties with data generated from the analytical formulation proposed by (BARRETO; PERES; PIRES, 2011),  $N_a = 4$  and  $N_e = 1000$ .

### 3.2.2

#### Dimensionless ES-MDA

The variables in the vector of model parameters may have different dimensions and variances. It could develop difficulty for the ES-MDA (RAFIEE; REYNOLDS, 2017). Normalization of the variables could be necessary. Preventing that, (ZHANG; REYNOLDS; OLIVER, 2002) formulated a dimensionless sensitivity matrix of the data:

$$G_d = C_d^{-1/2} G C_m^{1/2} \quad (3-29)$$

Note that the matrix  $\Delta M^k$  can be comprehended as the ensemble approximation of the square root of  $C_m$  at step  $k$ :

$$C_m \approx \Delta M^k (\Delta M^k)^T \quad (3-30)$$

$$C_m^{1/2} \approx \Delta M^k \quad (3-31)$$

Likewise, assuming the linear relation between model parameters and data, the following is achieved:

$$\Delta D^k = G \Delta M^k \quad (3-32)$$

Applying Equation (3-31) in Equation (3-29):

$$G_d^k \approx C_d^{-1/2} G \Delta M^k \quad (3-33)$$

Furthermore, using Equation (3-32) in the last equation:

$$G_d^k \approx C_d^{-1/2} \Delta D^k \quad (3-34)$$

Now the rewriting of Equation (3-22) is aimed using the dimensionless sensitivity matrix. Focusing on the term  $C_k = C_{md}^k(C_{dd}^k + \alpha_{k+1}C_d)^{-1}$ , it is possible to rewrite  $C_k$  using Equations (3-25) and (3-26):

$$C_k = \Delta M^k(\Delta D^k)^T(\Delta D^k(\Delta D^k)^T + \alpha_{k+1}C_d)^{-1} \quad (3-35)$$

Assuming  $C_d$  to be symmetric and knowing that  $C_d = C_d^{1/2}I_{N_d}C_d^{1/2}$ , where  $I_{N_d}$  is the  $N_d \times N_d$  identity matrix. The following is acquired:

$$\begin{aligned} C_k &= \Delta M^k(\Delta D^k)^T(C_d^{1/2}(C_d^{-1/2}\Delta D^k(\Delta D^k)^TC_d^{-1/2} + \alpha_{k+1}I_{N_d})C_d^{1/2})^{-1} \\ &= \Delta M^k(\Delta D^k)^TC_d^{-1/2}(C_d^{-1/2}\Delta D^k(\Delta D^k)^TC_d^{-1/2} + \alpha_{k+1}I_{N_d})^{-1}C_d^{-1/2} \end{aligned} \quad (3-36)$$

From Equation (3-34),  $(G_d^k)^T = (\Delta D^k)^TC_d^{-1/2}$ , and the right-hand size appears in Equation (3-36). Replacing this term:

$$C_k = \Delta M^k(G_d^k)^T(G_d^k(G_d^k)^T + \alpha_{k+1}I_{N_d})^{-1}C_d^{-1/2} \quad (3-37)$$

Replacing  $C_k$  computed in the ES-MDA updated equation is obtained the Dimensionless ES-MDA equation:

$$\delta m_j^{k+1} = (G_d^k)^T(G_d^k(G_d^k)^T + \alpha_{k+1}I_{N_d})^{-1}y_j^k \quad (3-38)$$

where  $\delta m_j^{k+1} = (\Delta M^k)^\dagger(m_j^{k+1} - m_j^k)$  is the dimensionless updated vector of parameters, and  $(\Delta M^k)^\dagger$  is the pseudo-inverse of  $\Delta M^k$ , and  $y_j^k = C_d^{-1/2}(d_{uc,j}^k - d_j^k)$  is the dimensionless vector of the data.

### 3.3

#### Inflation Factors Analysis

The ES-MDA has proven to be a promising method for history matching problems (EMERICK; REYNOLDS, 2013), but the main drawback is the designation of the number of assimilations  $N_a$ , and the inflation factors  $\{\alpha_k\}_{k=1}^{N_a}$  before the data assimilation. The most straightforward choice of inflation factors is to set them equal to  $N_a$ , but this selection might produce overcorrection among model parameters (LE; EMERICK; REYNOLDS, 2016).

Adaptive methods for calculating inflation factors during data assimilation were proposed to avoid this obstacle, such as in (LE; EMERICK; REYNOLDS, 2016), where two methods are presented, the ES-MDA-RS, using a predetermined level as a maximum quota for the model parameters and the ES-MDA-RLM, using the discrepancy principle, inspired by (HANKE, 1997) and (IGLESIAS; DAWSON, 2013).

Another alternative for adaptive ES-MDA algorithm was proposed on (IGLESIAS, 2014), using the same update equation of the ES-MDA, but the

choice of inflation factors is based on the discrepancy principle and is used as the stopping criterion.

Nevertheless, the number of assimilation in these procedures is unknown a priori, since it depends on stop criteria for calculating inflation factors. (RAFIEE; REYNOLDS, 2017) shows an example of when IR-ES fails to converge after more than 200 iterations. Moreover, (RAFIEE; REYNOLDS, 2017)s also showed cases that needed at least 20 assimilation steps to converge.

Since the increase of assimilations steps yields a run of the mathematical model presented in Chapter 2 for each ensemble member, it is crucial to minimize the number of assimilations for computational purposes. This thesis uses a procedure presented on (RAFIEE; REYNOLDS, 2017) to generate the inflation factors. One advantage is that the number of assimilation in this method can be assumed a priori, avoiding computational efficiency problems.

### 3.3.1

#### Inflation factor generation based on the discrepancy principle

This thesis uses the approach presented in (RAFIEE; REYNOLDS, 2017) to calculate inflation factors. The first inflation factor  $\alpha_1$  is calculated using the discrepancy principle. The following elements are calculated using a geometric descendance scheme based on the computation of  $\alpha_1$ .

Starting from Equation (3-38), setting  $k = 0$  (using the prior ensemble) one can update the mean of the model parameters  $m$  as:

$$\bar{m}^1 = \bar{m}^0 + \Delta M^0 (G_d^0)^T (G_d^0 (G_d^0)^T + \alpha_1 I_{N_d})^{-1} C_d^{1/2} (d_{obs} - \bar{d}^0) \quad (3-39)$$

One can notice that  $\bar{m}^1$  is the solution of the regularized least squares problem defined as

$$x^1 = \operatorname{argmin}_x \left\{ \frac{1}{2} \|G_d^0 x^0 - y^0\|^2 + \frac{\alpha_1}{2} \|x^0\|^2 \right\} \quad (3-40)$$

where

$$x = (\Delta M^k)^\dagger (\bar{m}^1 - \bar{m}^0) \quad (3-41)$$

and

$$y = C_d^{-1/2} (d_{obs} - \bar{d}^0) \quad (3-42)$$

Equation (3-41) represents the Tikhonov regularization method (RAFIEE; REYNOLDS, 2017) with regularization parameter  $\alpha_1$  used to the ill-posed problem:

$$G_d^0 x^0 = y^0 \quad (3-43)$$

The term  $\alpha_1$  controls the relevance of each term of sum in Equation (3-40). If  $\alpha_1$  is too large, both high and medium frequency components in the solution of Equation (3-41) are ruled out, and the solution may not be

physically viable. Meanwhile, if  $\alpha_1$  is too tiny, high-frequency components are included in the solution, and it is usually too oscillatory to be a tolerable solution. Here the discrepancy principle (VOGEL, 2002) is used to determine the optimum regularization parameter  $\alpha_1$ . It is straightforward to adopt that the data mismatch is greater than the noise level due to the data. Otherwise, there is no point in matching the data. So it is possible to write:

$$\|y\| > \eta \quad (3-44)$$

or

$$\|C_d^{-1/2}(d_{obs} - \bar{d}^0)\| > \eta \quad (3-45)$$

where  $\eta$  is the noise level defined as:

$$\eta^2 \equiv \|C_d^{-1/2}(d_{obs} - Gm_{true})\|^2 \quad (3-46)$$

Assuming that  $d_{obs} = Gm_{true} + \epsilon$ , where  $\epsilon \sim \mathcal{N}(0, C_d)$ ,  $\eta$  assumes a  $\chi^2$ -distribution with mean  $N_d$  (BARLOW, 1989). Thereby, it is acceptable (TARANTOLA, 2005) to assume  $\eta = \sqrt{N_d}$ . From Equation (3-43),  $(G_d^0 x_1 - y)$  is the difference between the regularized solution of Equation (3-39) and the data vector  $y$ . Therefore, the discrepancy principle says that the minimum regularization parameter  $\alpha_1$  should regard the following:

$$\eta = \|G_d^0 x_1 - y\| \quad (3-47)$$

Equation (3-47) has a unique solution for  $\alpha_1$  (GROETSCH, 1984). Using Equations (3-39) and (3-40) it is possible to depict the regularized solution of the inverse problem  $x_1$ :

$$x_1 = (G_d^0)^T (G_d^0 (G_d^0)^T + \alpha_1 I_{N_d})^{-1} C_d^{1/2} (d_{obs} - \bar{d}^0) \quad (3-48)$$

By Equations (3-48) and (3-42), it is possible to rewrite Equation (3-47):

$$\eta = \|G_d^0 x_1 - y\| = \alpha_1 \| (G_d^0 (G_d^0)^T + \alpha_1 I_{N_d})^{-1} C_d^{1/2} (d_{obs} - \bar{d}^0) \| \quad (3-49)$$

Using this expression for  $\eta$ , and replacing on Equation (3-44):

$$\|C_d^{-1/2}(d_{obs} - \bar{d}^0)\| > \alpha_1 \| (G_d^0 (G_d^0)^T + \alpha_1 I_{N_d})^{-1} C_d^{1/2} (d_{obs} - \bar{d}^0) \| \quad (3-50)$$

It is possible to obtain equality on (3-50) by multiplying the left-hand size by an appropriate constant  $\rho \in (0, 1)$ , yielding on:

$$\rho \|C_d^{-1/2}(d_{obs} - \bar{d}^0)\| = \alpha_1 \| (G_d^0 (G_d^0)^T + \alpha_1 I_{N_d})^{-1} C_d^{1/2} (d_{obs} - \bar{d}^0) \| \quad (3-51)$$

Therefore, Equation (3-51) states a relation between the approximation of

the norm of the dimensionless forecast data mismatch vector (term multiplied by  $\rho$ ). With a higher value of  $\rho$ , a slighter decrease in the data mismatch is achieved by more damping with a more significant value of  $\alpha_1$ . The following condition for the regularization parameter was proposed by (HANKE, 1997):

$$\rho^2 \|C_d^{-1/2}(d_{obs} - \bar{d}^0)\|^2 \leq \alpha_1^2 \|(G_d^0(G_d^0)^T + \alpha_1 I_{N_d})^{-1} C_d^{1/2}(d_{obs} - \bar{d}^0)\|^2 \quad (3-52)$$

It was shown that, for a stable solution of the inverse problem, it is sufficient to the regularization parameter to satisfy Equation (3-52). Below, we show how (RAFIEE; REYNOLDS, 2017) evaluates the right-hand side of Equation (3-52) using the SVD of  $G_d^0$ , yielding on a method to determine the minimum inflation factor that guarantees Equation (3-52).

Let  $U\Lambda V$  be the SVD decomposition of  $G_d^0$ . Where  $U \in \mathbb{R}^{N_d \times N_d}$  is an orthogonal matrix and its columns are the left singular vectors of  $G_d^0$ ,  $V \in \mathbb{R}^{N_e \times N_e}$  is an orthogonal matrix, and its columns are the right singular vectors of  $G_d^0$ , and  $\Lambda \in \mathbb{R}^{N_d \times N_e}$  is a matrix with all singular values of  $G_d^0$  in its diagonal entries. The singular values are ordered as:

$$\lambda_{max} \equiv \lambda_1 \geq \lambda_2 \geq \dots \geq \lambda_N \equiv \lambda_{min} \geq 0 \quad (3-53)$$

Where  $N$  is the minimum between  $N_d$  and  $N_e$ . Using the singular value decomposition, it is possible to write:

$$C \equiv G_d^0(G_d^0)^T + \alpha_1 I_{N_d} = (U\Lambda V^T)(U\Lambda V^T)^T + \alpha_1 I_{N_d} \quad (3-54)$$

Since  $U$  and  $V$  are orthogonal:

$$C \equiv U(\Lambda\Lambda^T + \alpha_1 I_{N_d})U^T \quad (3-55)$$

So the inverse of  $C$  is given by:

$$C^{-1} = U\Gamma U^T \quad (3-56)$$

Where  $\Gamma \in \mathbb{R}^{N_d \times N_d}$  diagonal matrix with its  $j$ th diagonal entry defined as:

$$\gamma_j = \frac{1}{\lambda_j^2 + \alpha_1} \quad (3-57)$$

Using Equation (3-42) and the definition of  $C$  given in (3-54), Equation (3-52) can be rewritten as:

$$\rho^2 \geq \alpha_i^2 \frac{\|C^{-1}y\|^2}{\|y\|^2} \quad (3-58)$$

Given that the columns of  $U$  form an orthonormal set,  $y$  can be interpreted as a linear combination of all column vectors of  $U$ :

$$y = \sum_{l=1}^{N_d} c_l u_l \quad (3-59)$$

where  $c_l$  are real scalars and  $u_l$  is the  $l$ th columns of  $U$  and since  $U$  is an orthogonal matrix:

$$\|y\|^2 = y^T y = \sum_{j=1}^{N_d} c_j^2 \quad (3-60)$$

In the same way,

$$\|C^{-1}y\|^2 = \left( \sum_{i=1}^{N_d} \gamma_i u_i c_i \right)^T \left( \sum_{i=1}^{N_d} \gamma_i u_i c_i \right) = \sum_{j=1}^{N_d} \gamma_j^2 c_j^2 \quad (3-61)$$

Replacing the results of Equations (3-60) and (3-61) on Equation (3-58):

$$\rho^2 \leq \alpha_1^2 \frac{\sum_{j=1}^{N_d} \gamma_j^2 c_j^2}{\sum_{j=1}^{N_d} c_j^2} \quad (3-62)$$

This equation can be solved numerically to obtain the value of  $\alpha_1$  that satisfies the discrepancy principle. The ratio on the right-hand side represents a weighted average of the squared eigenvalues of  $C^{-1}$ . If  $y$  is equal to constant times the  $k$ th eigenvector, then it is possible to rewrite the last equation as:

$$\rho^2 \leq \alpha_1^2 \gamma_k^2 = \frac{\alpha_1^2}{(\lambda_k^2 + \alpha_1)^2} \quad (3-63)$$

Or equivalent to:

$$\alpha_1 \geq \frac{\rho}{1 - \rho} \lambda_k^2 \quad (3-64)$$

In general, the largest value of  $\alpha_1$  that satisfies Equation (3-62) is achieved when  $y$  is parallel to the singular vector corresponding to the largest singular value and the smallest value of  $\alpha_1$  is obtained when  $y$  is aligned to the singular vector linked to the smallest singular value. So, the optimum value of  $\alpha_1$  is between these values. (RAFIEE; REYNOLDS, 2017) propose that  $\alpha_1$  should be computed as:

$$\alpha_1 = \frac{\rho}{1 - \rho} \bar{\lambda}^2 \quad (3-65)$$

where  $\bar{\lambda}$  is the mean of all singular values of  $G_d^0$  and it is calculate as:

$$\bar{\lambda} = \frac{1}{N} \sum_{j=1}^N \lambda_j \quad (3-66)$$

Where  $N$  is the number of non-zero singular values of  $G_d^0$ .

### 3.3.2

#### Geometric inflation factors generation

This subsection shows how (RAFIEE; REYNOLDS, 2017) calculates the ES-MDA inflation factors. One advantage of the following method is the

possibility of establishing the number of assimilations  $N_a$  *a priori*.

(RAFIEE; REYNOLDS, 2017) conjectured that selecting a low number of assimilations, e.g., from 4 to 8, with a proper selection of the inflation factors, would be enough to obtain good results when using the ES-MDA.

Given an initial condition, the first inflation factor  $\alpha_1$  is obtained using Equation (3-65), with  $\rho = 0.5$ . Therefore, one can compute  $\alpha_1$  as:

$$\alpha_1 = \bar{\lambda}^2 = \left( \frac{1}{N} \sum_{j=1}^N \lambda_j \right)^2. \quad (3-67)$$

The execution presented in (RAFIEE; REYNOLDS, 2017) of the IR-ES method (IGLESIAS, 2014) and the method used in (LE; EMERICK; REYNOLDS, 2016) indicate that the inflation factors usually decrease within the iterations of iterative ES. The results using the ES-MDA (LE; EMERICK; REYNOLDS, 2016) also suggest a drop in the calculated inflation factors. This thesis assumes they monotonically decrease with the rise of the index  $k$  representing the current assimilation step as in (EMERICK; REYNOLDS, 2013).

Considering a geometric generation of the inflation factors with geometric ratio  $\beta$ , one may compute  $\alpha_j$  as:

$$\alpha_j = \beta^{j-1} \alpha_1, \quad (3-68)$$

where  $\beta \in (0, 1)$ , and  $j = 1 \dots N_a$ . To evaluate the common ratio, Equation (3-68) is used in Equation (3-24):

$$\begin{aligned} \frac{1}{\beta^{j-1}} \frac{1}{\alpha_1} &= \frac{1}{\alpha_j} \\ \frac{1}{\alpha_1} \sum_{j=1}^{N_a} \frac{1}{\beta^{j-1}} &= \sum_{j=1}^{N_a} \frac{1}{\alpha_j} \\ \frac{1}{\alpha_1} \sum_{j=1}^{N_a} \frac{1}{\beta^{j-1}} &= 1 \\ \sum_{j=1}^{N_a} \frac{1}{\beta^{j-1}} &= \alpha_1. \end{aligned} \quad (3-69)$$

The well-known summation of the geometric sequence is used in Equation (3-69) to achieve

$$\frac{1 - \left(\frac{1}{\beta}\right)^{N_a-1}}{1 - \frac{1}{\beta}} = \alpha_1. \quad (3-70)$$

Equation (3-70) can be solved for  $\beta \in (0, 1)$ . With the value of  $\beta$ , all inflation factors can be calculated using Equation (3-68).

In summation, the method for calculating the inflation factors proposed by (RAFIEE; REYNOLDS, 2017) allows the specification of the number of

data assimilation  $N_a$  and generates the first inflation factor  $\alpha_1$  using Equation (3-67). The common ratio  $\beta$  can be computed using Equation (3-70). Finally, the inflation factors can be computed using Equation (3-68). The pseudo-code of the ES-MDA-GEO is presented below.

1. Choose the number of data assimilation  $N_a$  and number of ensembles  $N_e$ .
2. Calculate the initial ensemble  $\{m_j^0\}_{j=1}^{N_e}$ .
3. Calculate the inflation factors  $\{\alpha_i\}_{i=1}^{N_a}$  as follow:
  - (a) Evaluate  $\Delta D^0$  as defined in (3-28) and the dimensionless sensitivity matrix  $G_d^0$  as defined in (3-34).
  - (b) Compute  $\alpha_1$  using Equation (3-67).
  - (c) Compute  $\beta$  using equation (3-70).
  - (d) Calculate the remaining inflation factors using Equation (3-68).
4. For  $i = 0 \dots N_a - 1$ 
  - (a) If  $i > 0$ 
    - i. Run the ensemble from time zero.
    - ii. Evaluate  $\Delta D^i$  as defined in Equation (3-28).
    - iii. Compute  $G_d^i$  using Equation (3-34).
  - (b) Evaluate  $\Delta M^i$  as in Equation (3-27).
  - (c) For  $j = 1 \dots N_e$ 
    - i. Perturb the observation vector using  $d_{ucj}^i = d_{obs} + \sqrt{\alpha_i C_d^{1/2}} z_j^i$ , with  $z_j^i \sim \mathcal{N}(0, I_{N_d})$ .
  - (d) End for
  - (e) Update the vector of model parameters using Equation (3-38)
5. End for

## 4 Results

The dimensionless ES-MDA was applied in a series of cases to test the conformity of the mathematical method presented in Chapter 2. Except for the permeability and skin zone radius and permeability used as the parameter model, all other reservoir parameter was given as constant in all cases.

The cases presented here are based on (SILVA et al., 2021), but the data estimated here cover the skin factor and the permeability and radius of the skin zone individually. Furthermore, there is also an estimate for the permeability of the layer.

In the work of (SILVA et al., 2021), pressure data were calculated using the model developed by (BARRETO; PERES; PIRES, 2011). On the other hand, in this work, the formulation developed by (VIANA et al., 2022) was used. Although this model assumes a piston-like water displacement, it allows the flow rate data in each layer to be calculated (BELA; PESCO; BARRETO, 2022).

### 4.1 Proposed Methodology

In Chapter 2, we presented a mathematical formulation to evaluate each layer's pressure difference and flow-rate. To increase uncertainty, artificial Gaussian noise was added to the pressure data to simulate a more realistic field case condition since, in an actual field injectivity test, pressure measurement is usually noisy due to measurement errors such as tidal effects (SILVA et al., 2021). Besides, only a few entrances of the observed flow-rate data were considered since, in a realistic field, the flow-rate data is hard to calculate all the time.

Subsequently, the pressure difference and flow-rate responses are considered the observed data in the dimensionless ES-MDA. This thesis uses the dimensionless ES-MDA because of the significant difference between the magnitudes within the observed data of pressure difference and flow-rate response.

Each Layer's permeability, skin zone radius, and skin zone permeability were chosen as model parameters for the dimensionless ES-MDA. In this study, we consider the number of ensembles  $N_e = 1000$  and the number of assimilations  $N_a = 4$  as suggested by (SILVA et al., 2021).

Oil properties were considered to be the same in all layers. A piston-like water displacement is assumed, and the water injection is supposed to last ten

hours. Fluid and rock information are shown in Table 4.1.

| $c_r$ (cm/kgf)       | $c_w$ ( $cm^2/kgf$ ) | $c_o$ ( $cm^2/kgf$ ) | $\mu_w$ (cP) | $r_w$ (m) |
|----------------------|----------------------|----------------------|--------------|-----------|
| $8.00 \cdot 10^{-5}$ | $4.04 \cdot 10^{-5}$ | $1.14 \cdot 10^{-4}$ | 0.52         | 0.108     |

Table 4.1: Table for Input parameters

The initial ensemble was set up such that a random vector of skin zone radius was created. This vector sorts normally distributed values between 0.108 m and 1.5 m. All along the data assimilation, the logarithm transformation of layer permeability and skin zone permeability is used since we assume the measurements are Gaussian. Therefore, they are sorted from a normally distributed range that varies according to the individual layer permeabilities and skin zone permeabilities. The initial guess for each layer skin zone permeability lower limit is 10 mD, and the upper limit consists of 1000 mD. For the layer permeability, the lower limit is 50 mD, and the upper limit consists of 5000 mD.

Table 4.2 portrays all case properties for each layer. Note that the skin zone radius is assumed to be the sum of the skin zone length and  $r_w$ . For all cases, the presented results include a graph of the observed data pressure difference response, the initial ensemble computed, and the final ensemble evaluated. The mean of the final ensemble also was displayed. Furthermore, the derivative is also displayed, and during an injectivity test, a characteristic signature may be identified if there is a formation damaged. Nevertheless, in this thesis, we added a Gaussian noise that may impair the characteristic signature.

Moreover, a graph for the observed data flow-rate response is presented. Also, both initial and final ensembles are displayed. Even though there is no practical interpretation of the final ensemble mean, it is shown, providing a visual representation of how, as a whole, the final ensemble represents the observed flow-rate. For all cases, each parameter estimated has a histogram graph comparing the initial ensemble, the final ensemble, and the actual value of the parameter.

| Case     | $q_{inj}$   | $\phi$ | $\mu_0$ | Layer | $k_j$         | $h_j$         | $k_{j_{skin}}$ | $r_{j_{skin}}$       |
|----------|-------------|--------|---------|-------|---------------|---------------|----------------|----------------------|
|          | ( $m^3/d$ ) |        |         |       | ( <b>cP</b> ) | ( <b>mD</b> ) | ( <b>m</b> )   | ( <b>mD</b> )        |
| <b>A</b> | 500         | 0.32   | 5.1     | 1     | 1000          | 10            | 500            | 0.408 ( $0.3+r_w$ )  |
|          |             |        |         | 2     | 1000          | 15            | 100            | 0.608 ( $0.5+r_w$ )  |
| <b>B</b> | 200         | 0.12   | 1.0     | 1     | 600           | 10            | 240            | 0.358 ( $0.25+r_w$ ) |
|          |             |        |         | 2     | 600           | 10            | -              | -                    |
| <b>C</b> | 400         | 0.15   | 1.5     | 1     | 1000          | 10            | 250            | 0.508 ( $0.4+r_w$ )  |
|          |             |        |         | 2     | 1200          | 8             | 400            | 0.608 ( $0.5+r_w$ )  |
|          |             |        |         | 3     | 800           | 7             | 300            | 0.308 ( $0.2+r_w$ )  |
| <b>D</b> | 100         | 0.25   | 2.3     | 1     | 600           | 15            | 150            | 0.308 ( $0.2+r_w$ )  |
|          |             |        |         | 2     | 800           | 10            | 200            | 0.308 ( $0.2+r_w$ )  |

Table 4.2: Table for all Cases Properties

## 4.2

### Case A

Case A portrays a two-layer reservoir with the same permeability on both layers but different skin zone properties. The oil viscosity is greater than the water one, and a porosity of 32% is considered, as shown in Table 4.2. Results for case A are shown in Figure 4.1 to 4.8. The pressure variation response (Figure 4.1) at the final ensemble is significantly more narrowed than the initial one. Likewise, the final ensemble range is substantially close to the observed data. This behavior corroborates that ES-MDA returned good results for each layer with damaged zone properties.

The derivative demeanor in Figure 4.1 seems unstable. This is explained by the noise included in pressure behavior. Since the derivative is calculated using the Stehfest Algorithm (STEHFEST, 1970) that uses the pressure information, the noise included reverberates on the derivative behavior.

Furthermore, the same demeanor appears on the flow-rate response (Figure 4.2). The initial ensemble is more spread than the final ensemble, which appears to converge to the observed data. It endorses that the Dimensionless ES-MDA had dealt well with the vast magnitude difference between pressure variation and flow-rate.

In case A, only the flow-rate for Layer 1 was estimated. This choice was made because, in case A, there are only two layers, and the flow-rate on the second layer at any particular time will be the difference between the flow-rate injection and the value estimated for layer 1. This is a direct consequence of the mass conservation principle, considered in the mathematical formulation

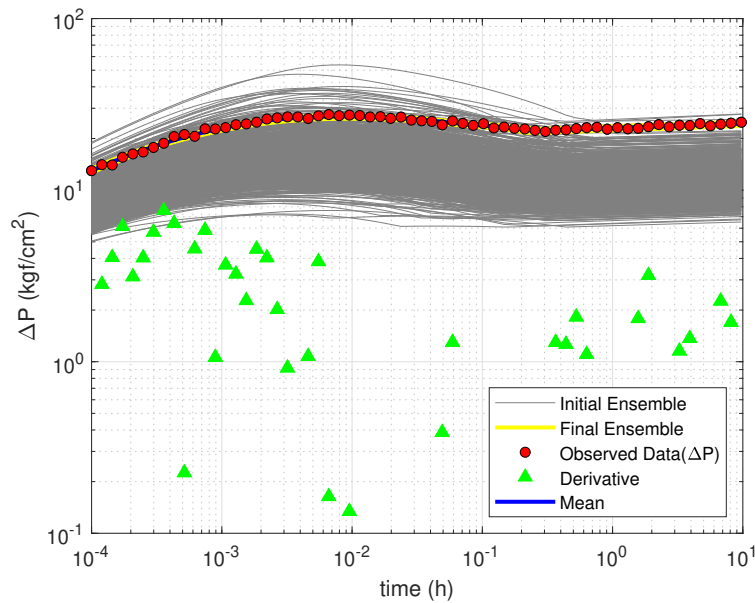


Figure 4.1: Pressure response for case A

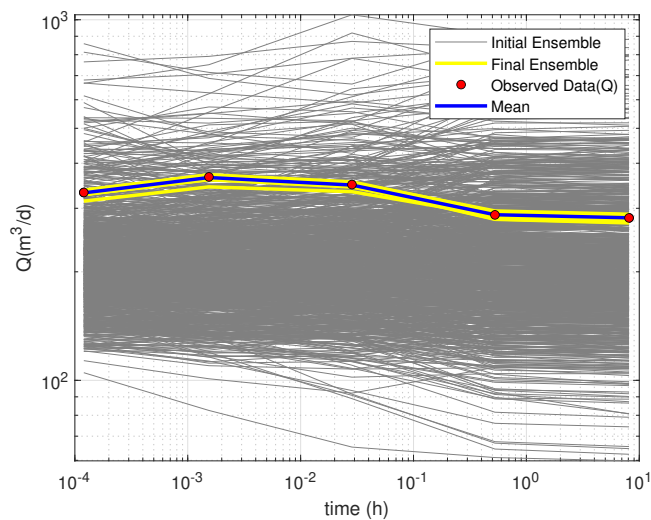


Figure 4.2: Flow-Rate response on layer 1 for case A

in Chapter 2.

The diagrams in Figures 4.3 and 4.4 depict the skin zone permeability estimations for layers 1 and 2, respectively. In both cases, it is possible to observe a convergence. Even though there is a slight error comparing the actual and estimated values, this can be explained by the complexity of the problem, and in both layers, the actual value is inside the final ensemble histogram.

The skin zone radius histograms for layer 1 and 2 (Figures 4.5 and 4.6) shows that the estimated values frequently got close to the actual value. Overall, the results for both layers indicate a good conversion towards the reservoir skin zone radius.

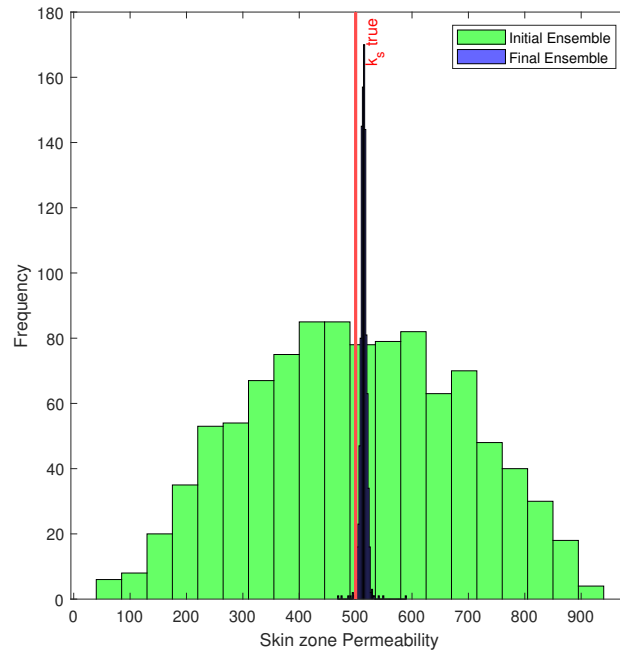


Figure 4.3: Permeability of the damaged zone histogram on layer 1 for case A

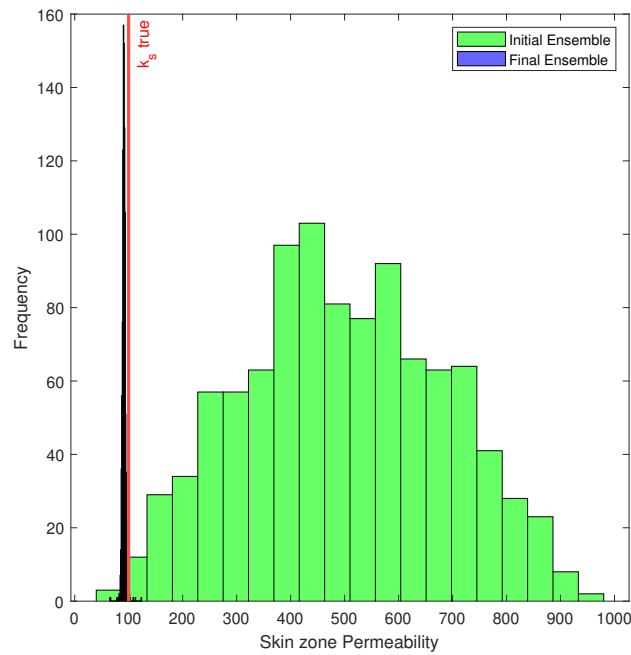


Figure 4.4: Permeability of the damaged zone histogram on layer 2 for case A

The histograms in Figures 4.7 and 4.8 correspond to both layers' estimative permeabilities. It indicates an explicit cramped range conversion at the final ensemble to the actual value estimated. Altogether, the results for both layers suggest that ES-MDA converges toward the reservoir's permeability.

It is possible to see that the insertion of a flow-rate response as data for the ES-MDA increases the estimation accuracy for each layer's properties.

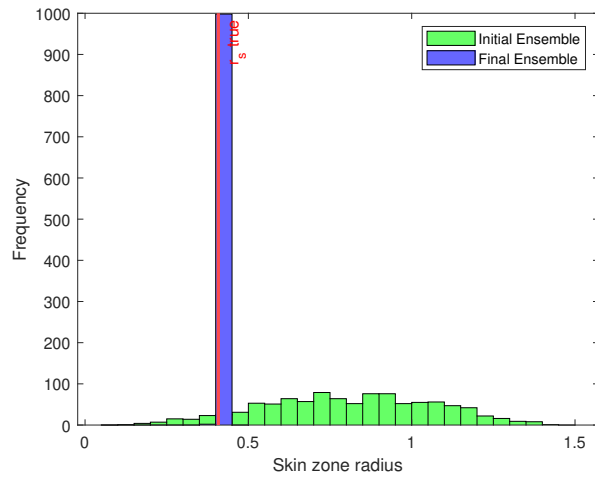


Figure 4.5: Radius of the damaged zone histogram on layer 1 for case A

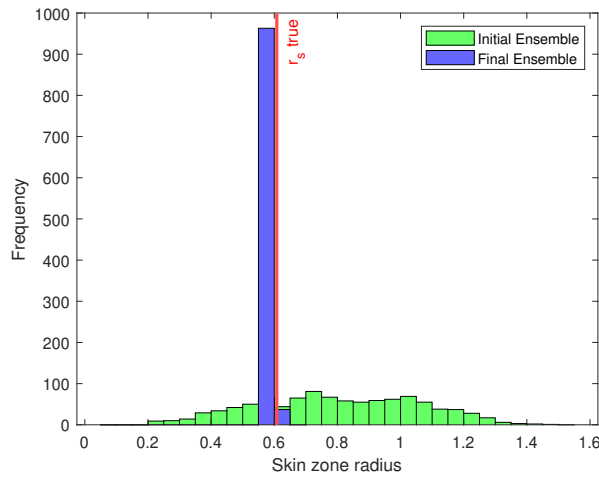


Figure 4.6: Radius of the damaged zone histogram on layer 2 for case A

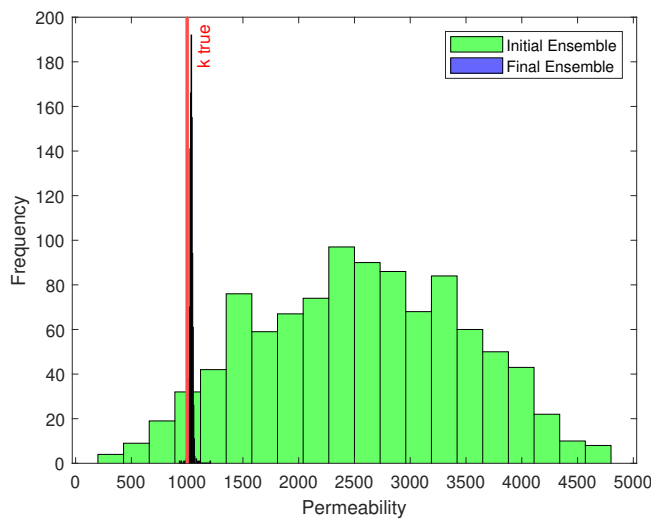


Figure 4.7: Permeability histogram on layer 1 for case A

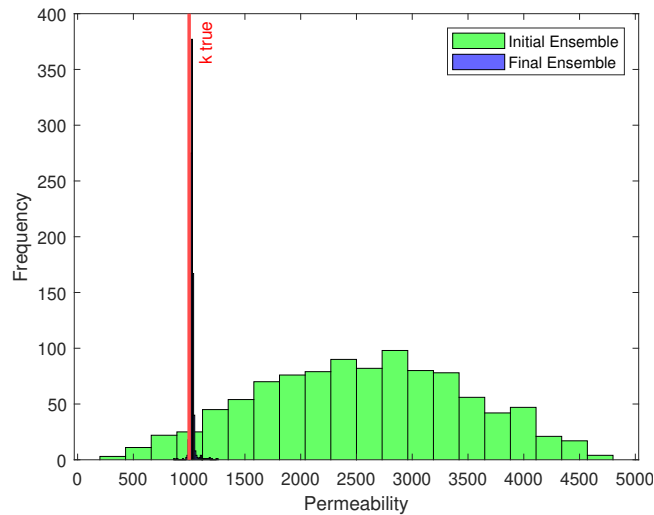


Figure 4.8: Permeability histogram on layer 2 for case A

Even the individual skin zone properties that, due to the problem's complexity, are sometimes calculated with the skin factor that correlates both radius and permeability on the same value, as in (SILVA et al., 2021), had good estimation values, close to the actual ones and presenting a sharp conversion.

### 4.3 Case B

Case B describes a two-layer reservoir with the same permeability and layer thickness on both layers but different skin zone properties. Only the first layer has a damaged zone in this case, and a porosity of 12% is considered, as shown in Table 4.2.

Results for case B are shown in Figure 4.9 to 4.16. As in case A, the final ensemble for pressure variation response (Figure 4.9) appears to tighten much more than the initial one. Besides, it appears to have an excellent conversion to the observed data, endorsing the idea that ES-MDA had dealt well with the estimation for each layer's properties.

Once again, the pressure variation derivative conduct (green triangles in Figure 4.9) seems unstable. And as explained for case A, the noise added on case B data causes this type of behavior since Stehfest Algorithm (STEHFEST, 1970)) is used.

In addition, the flow-rate response estimation (Figure 4.10) had good results. The final ensemble is much more narrow than the initial one and coincides with the observed data. Once more, the ES-MDA appears to have handled the considerable difference of magnitude within the input data.

The histograms for skin zone permeabilities (Figures 4.11 and 4.12)

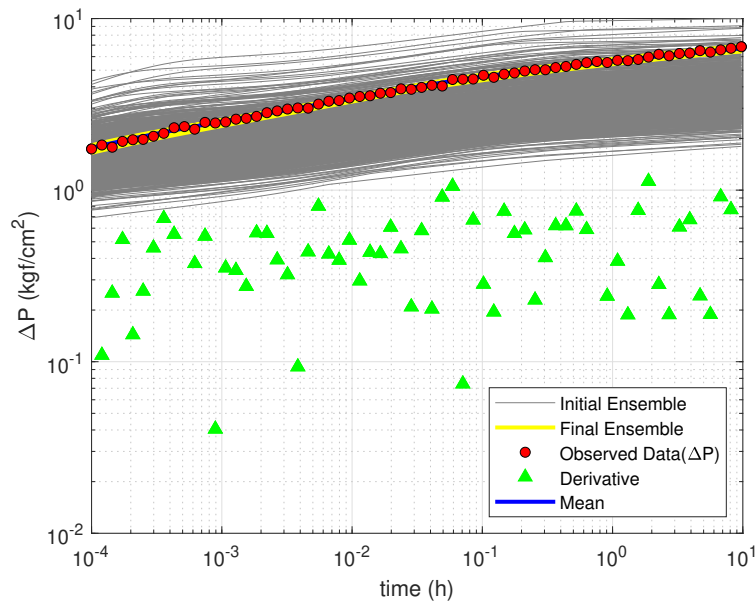


Figure 4.9: Pressure response for case B

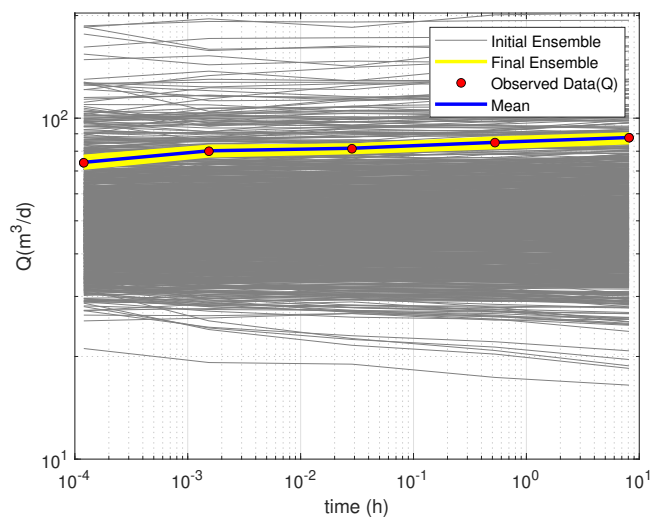


Figure 4.10: Flow-Rate response on layer 1 for case B

illustrate the skin zone permeability evaluations for layers 1 and 2. For layer 1, it is possible to see a good conversion since the histogram is threadlike and appears to assemble to the actual value of the skin factor permeability. For layer 2, since there is no damaged zone, the actual permeability is the permeability for layer 2. Considering that the real value is inside the histogram that seems to have a good conversion, good results were obtained.

The skin zone radius histogram for layer 1 (Figure 4.13) shows that the estimated values are frequently near the actual value. The outcomes for layer 1 indicate good conversion since the initial ensemble histogram is much more spread than the final one and gives the impression that it coincides with

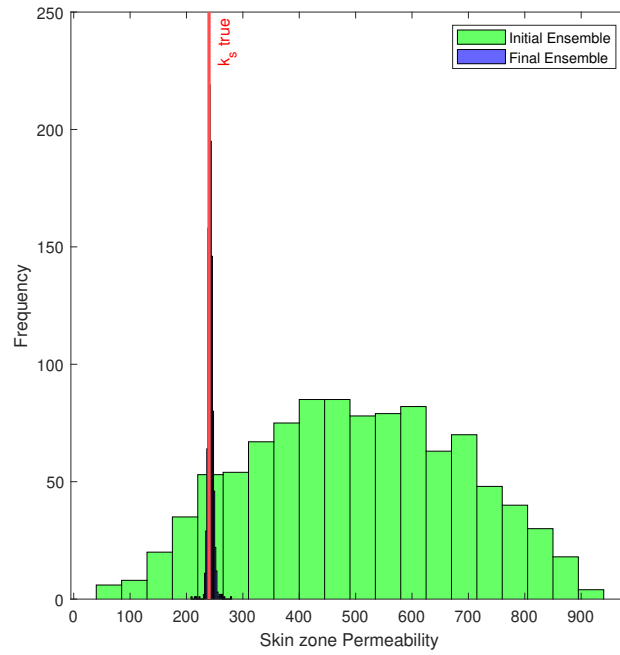


Figure 4.11: Permeability of the damaged zone histogram on layer 1 for case B

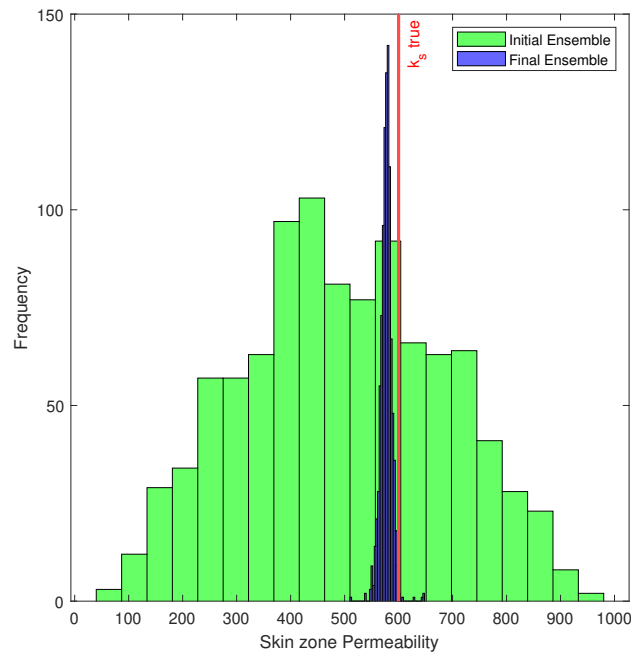


Figure 4.12: Permeability of the damaged zone histogram on layer 2 for case B

the skin zone radius.

In layer 2, there is no skin zone, so its radius is zero. Nevertheless, since an initial ensemble was provided as an input for the ES-MDA, the algorithm will try to converge to a value inside it. Therefore, since the option of the radius being empty on the initial ensemble is not considered, the ES-MDA will converge to a possible value on the initial ensemble, and the demeanor

shown in Figure 4.14 is plausible. Despite not interfering with  $\Delta p$ , since the permeabilities for the skin zone are suitable. It can be a consequence of spurious correlations, they can be improved with localization techniques, but in this particular problem that is complex.

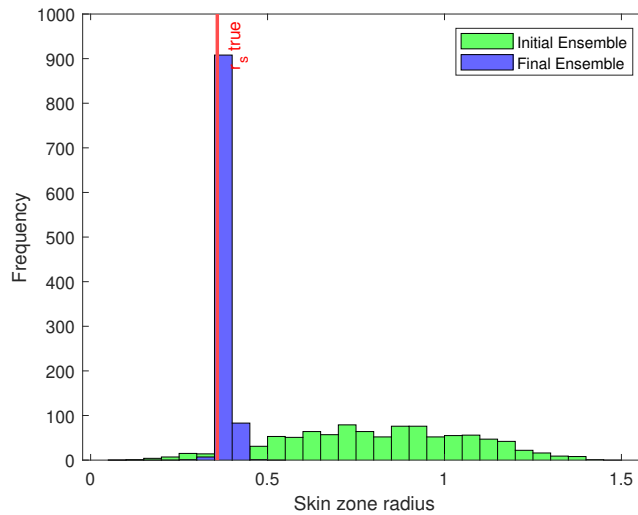


Figure 4.13: Radius of the damaged zone histogram on layer 1 for case B

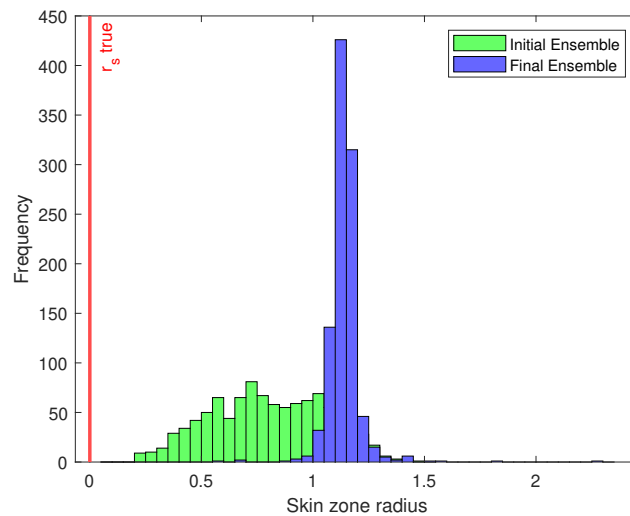


Figure 4.14: Radius of the damaged zone histogram on layer 2 for case B

The outcomes for both layers' permeabilities estimation are pointed out in Figure 4.15 and Figure 4.16. In general, the two final ensembles seem to have a sharpened conversion, and in both cases, the results appear to be synergistic with the actual values for each layer's permeability.

Thus, the results obtained for case B seem to describe the reservoir properties well. Altogether, ES-MDA had good results handling a reservoir with a layer without a damaged zone. Including a few flow-rate data as an input suggests a good aid for the outcomes.

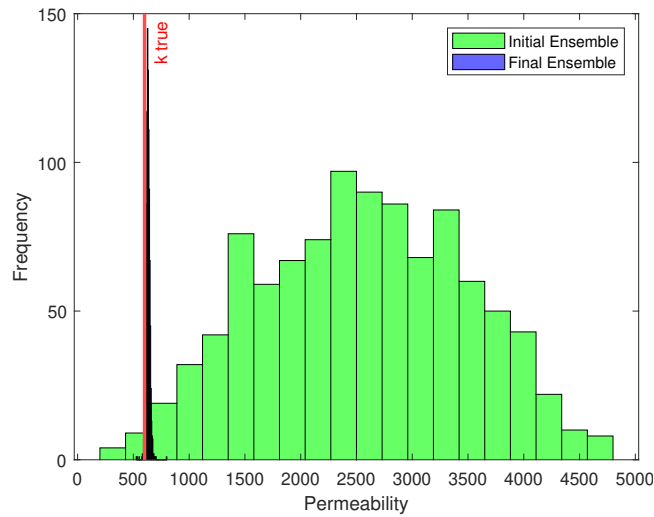


Figure 4.15: Permeability histogram on layer 1 for case B

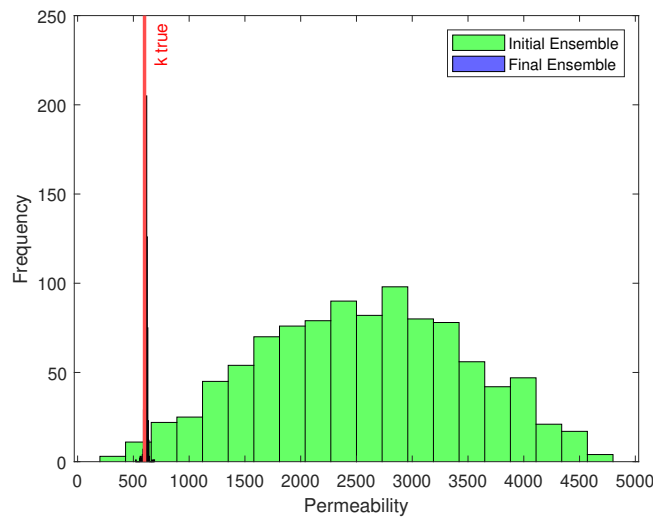


Figure 4.16: Permeability histogram on layer 2 for case B

#### 4.4

##### Case C

Case C illustrates a three-layer reservoir with different permeabilities and skin zone properties on all layers. The complexity of the problem is increased since more layers are taken into account, and a porosity of 15 % is considered, as shown in Table 4.2.

Results for case C are shown in Figure 4.17 to 4.27. The pressure variation response (Figure 4.17) shows a good demeanor for the final ensemble. It matches the observed data and is more controlled than the initial one. The results ratified that ES-MDA transmitted each layer's properties, even with an extension of the complexity of the problem, adding one more layer.

Moreover, since there are three layers, in this case, estimating the flow-

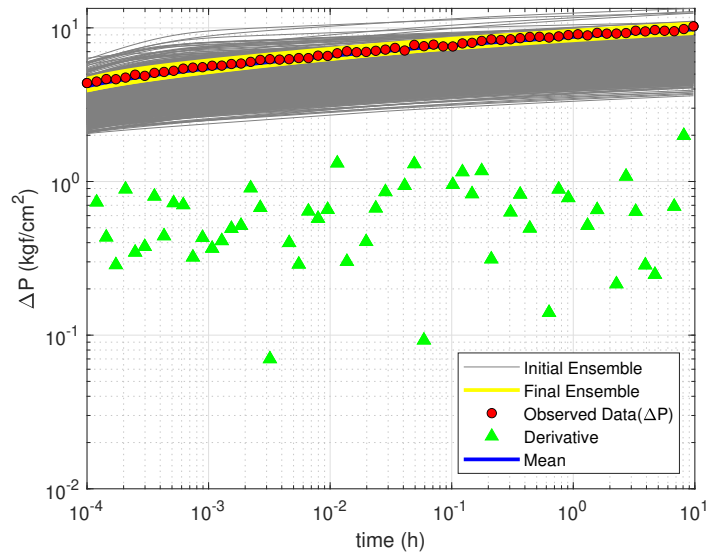


Figure 4.17: Pressure response for case C

rate response for two of them is reasonable. Here, we choose to calculate the flow-rate response for layers one and two. With the same argument presented in case A, it is not helpful to estimate the third layer since it is possible to calculate using the first two, using the mass conservation principle.

The flow-rate response for layers one and two are presented in Figure 4.18 and Figure 4.19. On the whole, the assimilation yielded good results for both layers. As in the pressure variation response, the final ensemble on each layer is much more narrowed than the initial one. Besides, it seems to suit the observed data for both layers.

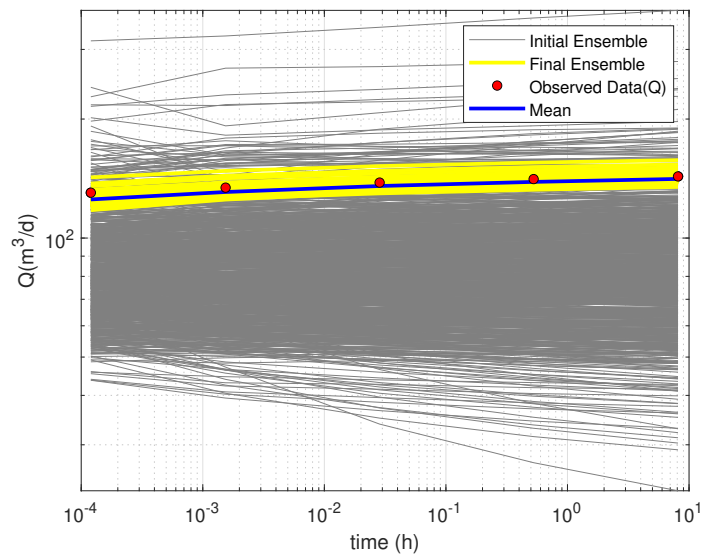


Figure 4.18: Flow-Rate response on layer 1 for case C

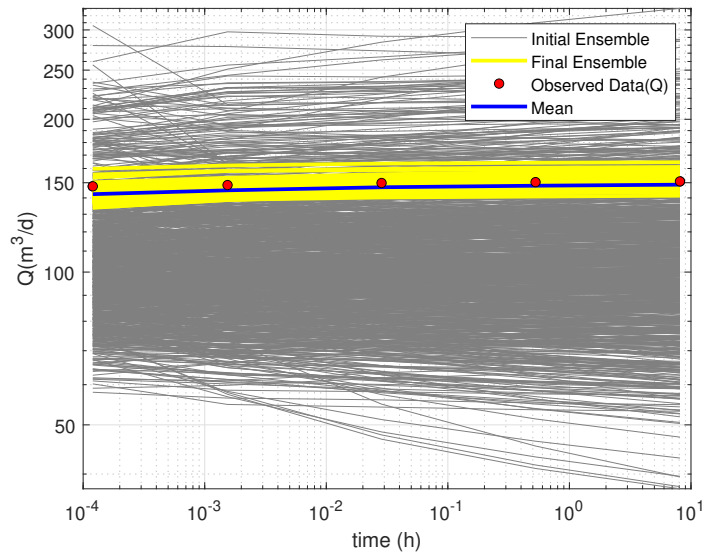


Figure 4.19: Flow-Rate response on layer 2 for case C

The histograms in Figures 4.20, 4.21, and 4.22, sketch the skin zone permeability estimation for all three layers. The final ensemble seems to converge on all situations since the histogram its histogram is much more limited than the initial one. Despite a modest error comparing the actual value and the one to which the ensemble converges on layers one and two, the real value is inside the final ensemble histogram for both cases.

Moreover, it is possible to observe that, whereas, on layers one and two, the final ensemble is slightly more spread for the third layer (Figure 4.22). The increased complexity of the problem could explain this demeanor. Since more parameters are estimated, some of them may be evaluated with more extended possible values.

Interestingly, despite a more widespread histogram for the final ensemble on layer three, it seems to converge to the actual value of the third layer skin zone permeability. This fact sustains that ES-MDA had dealt well with the increase in complexity of the problem.

Overall, the skin zone permeability outcomes when adding a new layer were good. Besides, it is possible to observe a good conversion for the value on the third layer. In all situations, the actual value is inside the final ensemble histogram.

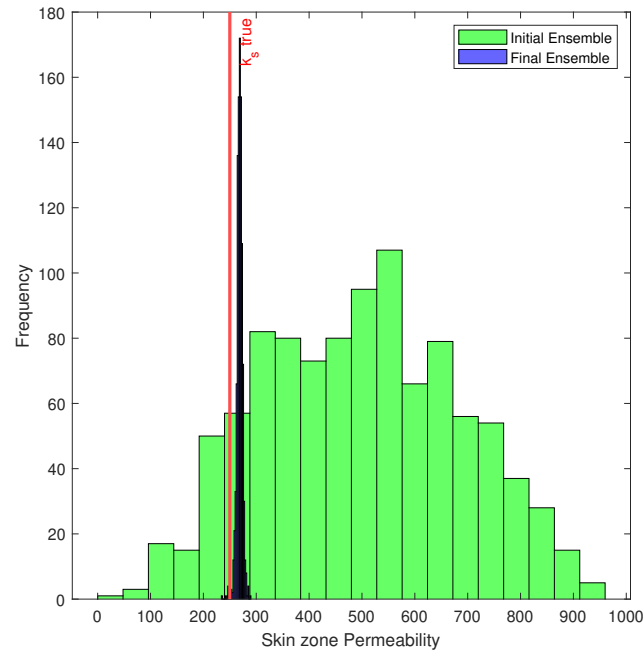


Figure 4.20: Permeability of the damaged zone histogram on layer 1 for case C

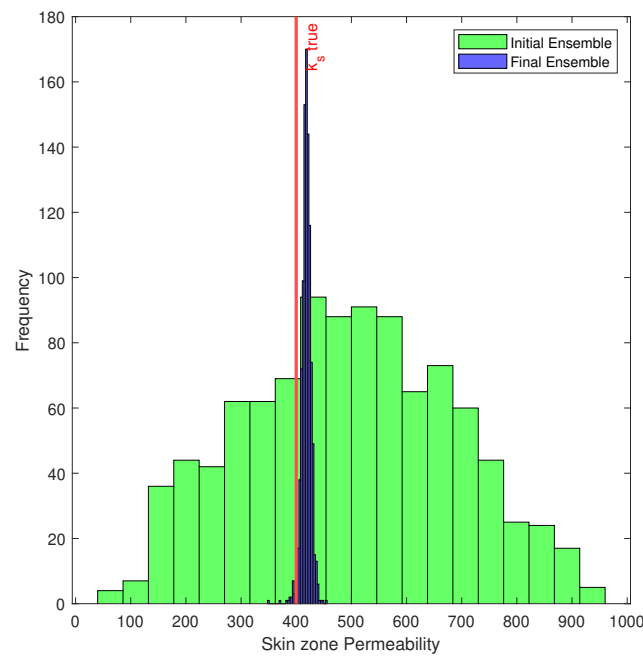


Figure 4.21: Permeability of the damaged zone histogram on layer 2 for case C

The skin zone radius histograms for all layers (Figures 4.23, 4.24, and 4.25) yielded good results on the final ensemble. For the three cases, the outcomes seem to converge toward the actual values, and the histogram is way more restricted than the initial one.

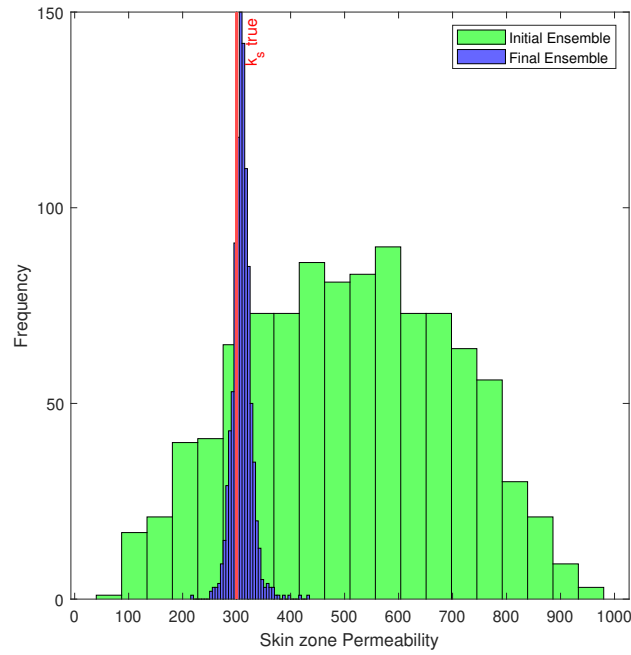


Figure 4.22: Permeability of the damaged zone histogram on layer 3 for case C

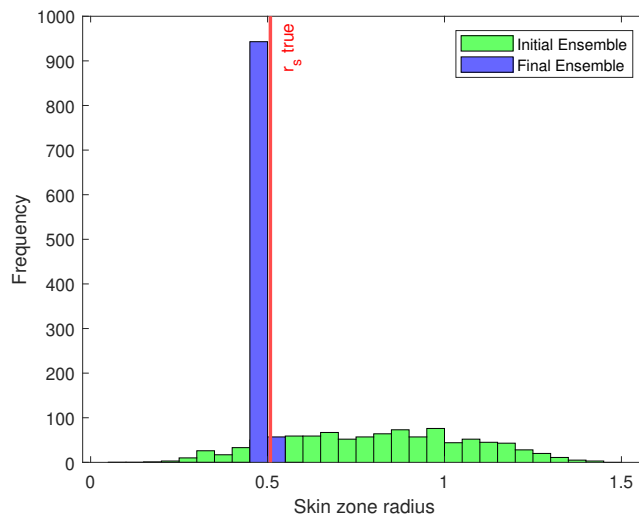


Figure 4.23: Radius of the damaged zone histogram on layer 1 for case C

Similar to the skin zone permeability demeanor, on the third layer (Figure 4.25), the final ensemble histogram for the skin zone radius is more spread than the other two. Once again, the amplification of the complexity of the problem, adding more parameters, and increasing the non-linearity explain this type of behavior.

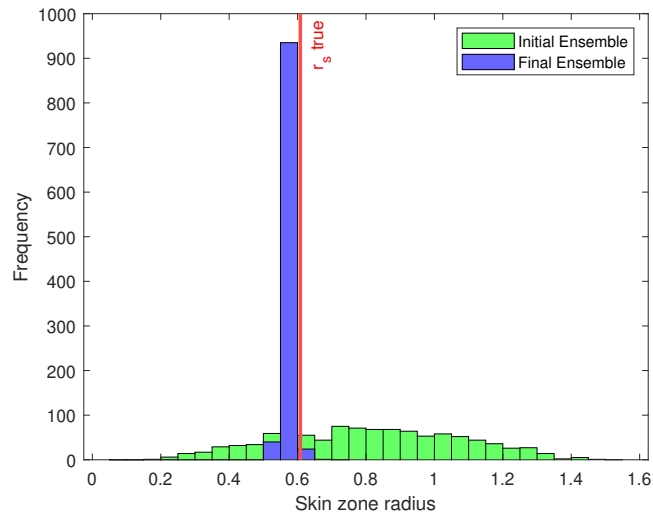


Figure 4.24: Radius of the damaged zone histogram on layer 2 for case C

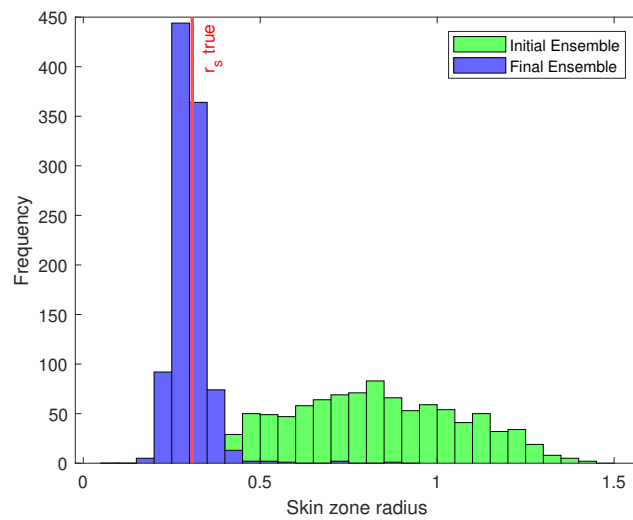


Figure 4.25: Radius of the damaged zone histogram on layer 3 for case C

The skin zone radius results when adding a new layer were generally good. Further, the third layer radius outcome presented an excellent conversion to the real value. In all situations, the actual radius is inside the final ensemble histogram.

The histograms in Figures 4.26, 4.27, and 4.28 correspond to all layers' estimative permeabilities. The final ensemble outcomes for the three situations depict a good demeanor, with a shorter range than the initial one.

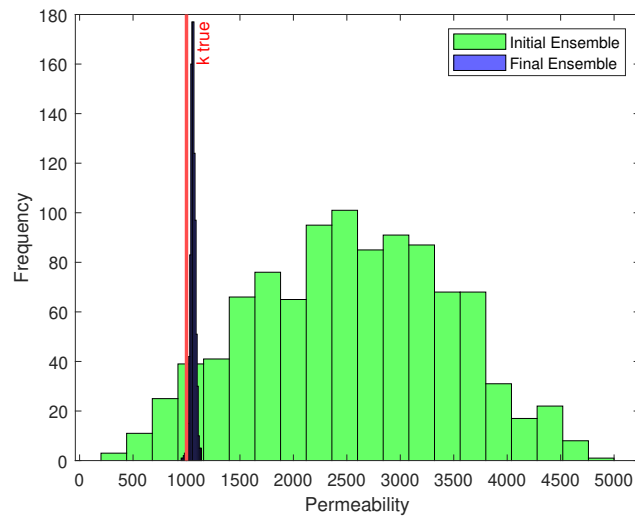


Figure 4.26: Permeability histogram on layer 1 for case C

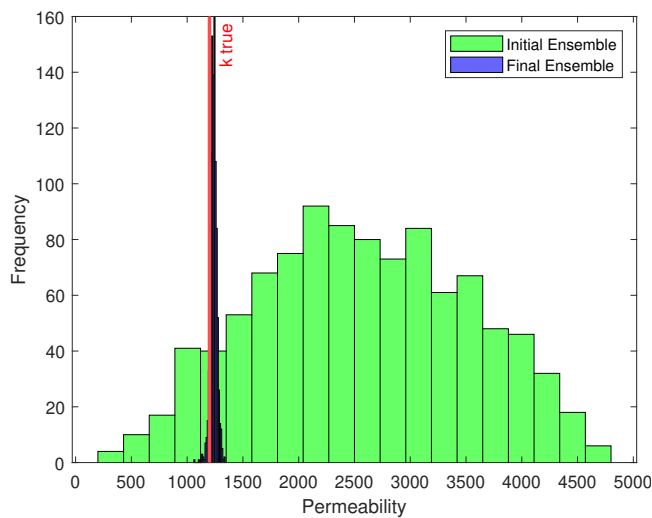


Figure 4.27: Permeability histogram on layer 2 for case C

On the third layer permeability estimation (Figure 4.28), it is possible to notice a feeble error comparing the actual value and the one in which the final ensemble converges. Nonetheless, this behavior is plausible due to the rise of entanglement of the problem, adding another layer. Moreover, the actual value is inside the final ensemble histogram.

Therefore, good results were acquired in case C. Naturally, drawbacks appear due to the additional layer. Nevertheless, ES-MDA appears to handle well the additional parameters estimated.

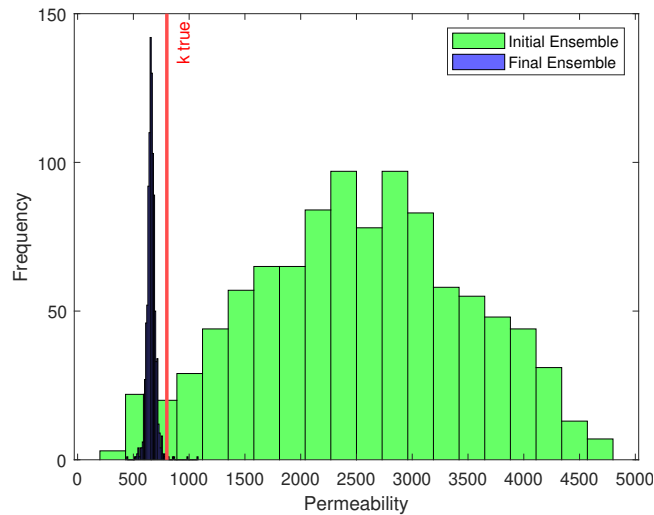


Figure 4.28: Permeability histogram on layer 3 for case C

#### 4.5 Case D

Case D consists of a two-layer reservoir where layer properties differ, but skin factors and radius are the same. Thus, the waterfront overcomes the damaged zone in each layer approximately simultaneously.

Results for case D are shown in Figure 4.29 to 4.36. The Pressure variation response (Figure 4.29) at the final ensemble presents a threadlike demeanor, being more limited than the initial one. Also, the final ensemble seems to agree well with the observed data. In (SILVA et al., 2021), part of the final ensemble in this case was unstable, possibly due to the similarity between layer skin zone radius. Thereby, adding the flow-rate as observed data for ES-MDA seems to aid in the stability of this case.

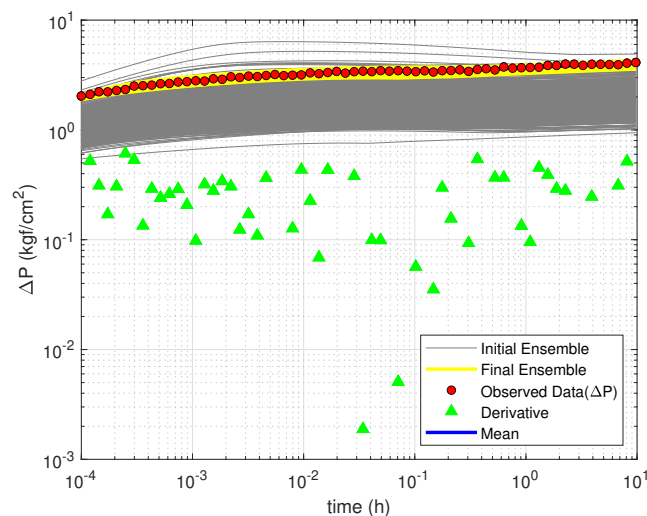


Figure 4.29: Pressure response for case D

On flow-rate response for this case (Figure 4.30), as in the others, the initial ensemble is more dispersed than the final one. Moreover, the final ensemble seems to match the observed data. The ES-MDA appears to have no problem of instability to fit the observed data, which could occur due to the configuration of the problem or the difference between flow-rate and pressure variation magnitude

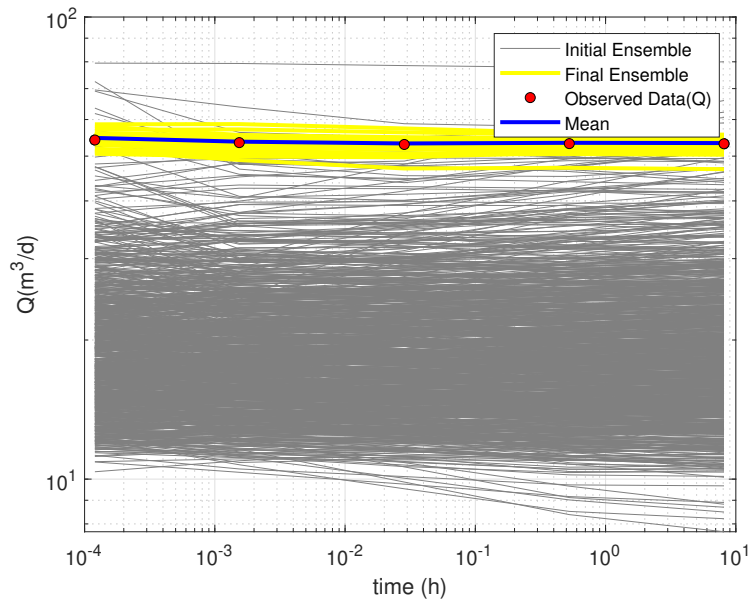


Figure 4.30: Flow-Rate response on layer 1 for case D

The skin zone permeability outcomes for both layers are presented in Figure 4.31 and Figure 4.32. In the two situations, it is possible to notice conversion on the final ensemble histogram. Despite a slight error contrasting the value that the final ensemble converges and the actual one in both cases, for the two layers, the real value is inside the final histogram.

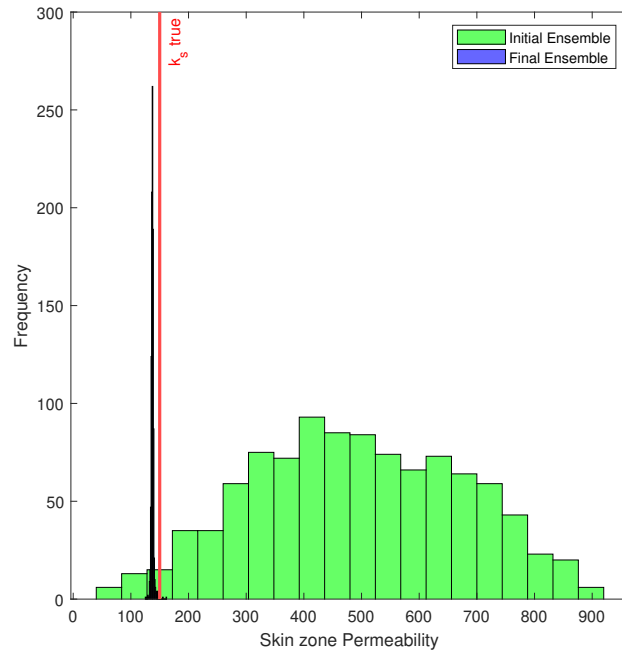


Figure 4.31: Permeability of the damaged zone histogram on layer 1 for case D

PUC-Rio - Certificação Digital N° 1912780/CA

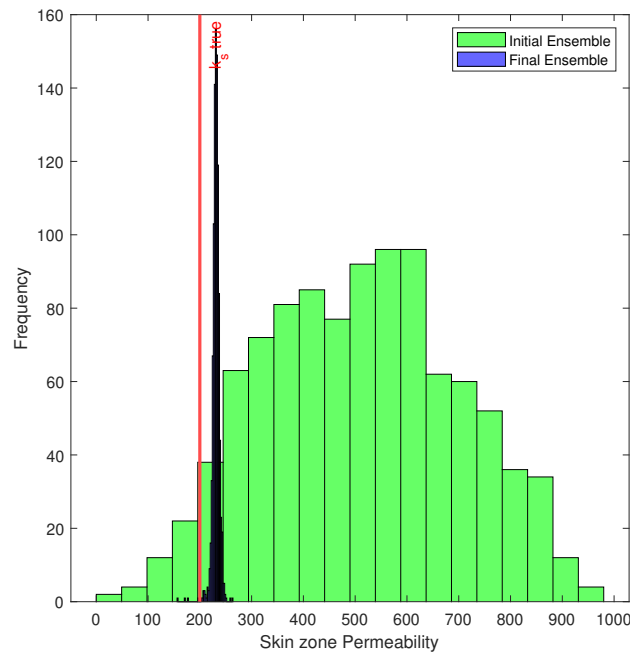


Figure 4.32: Permeability of the damaged zone histogram on layer 2 for case D

The skin zone radius values estimated for each layer in case B are presented in Figure 4.13 and Figure 4.14. It is possible to observe a high frequency near the actual value in both scenarios. The outcomes for the two layers indicate a conversion to the true values of the skin zone radius.

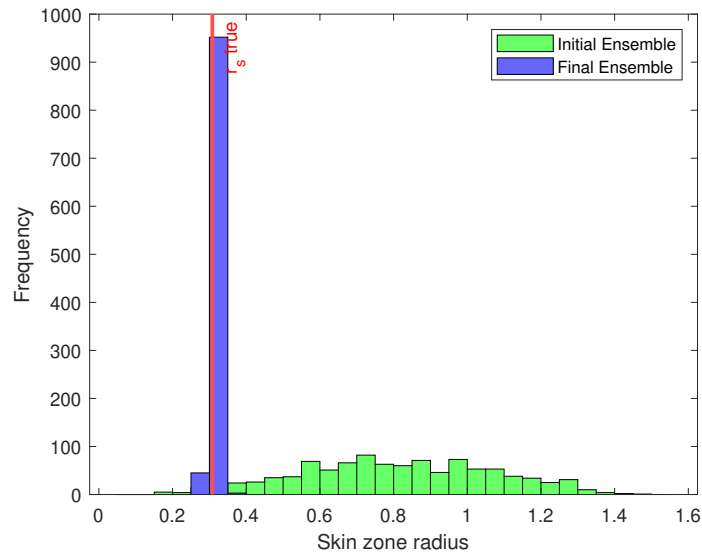


Figure 4.33: Radius of the damaged zone histogram on layer 1 for case D

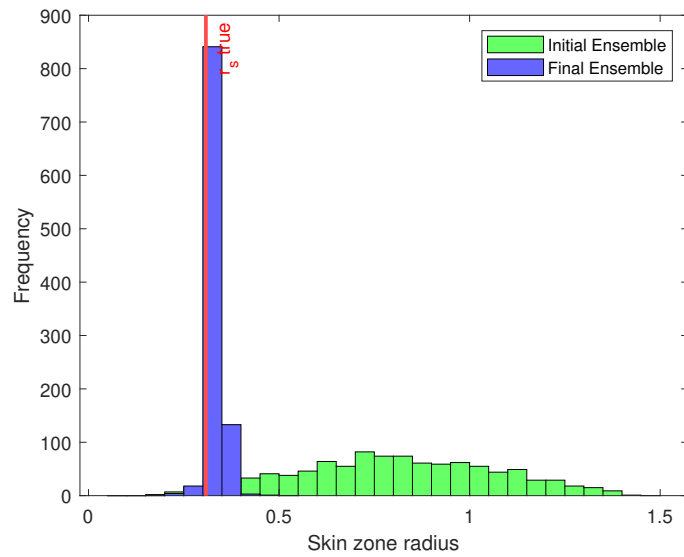


Figure 4.34: Radius of the damaged zone histogram on layer 2 for case D

The histograms in Figures 4.35 and Figure 4.36 portray both layers' estimative permeabilities. The final ensemble seems to converge on both situations, with a narrow range. On both layers, the real value is inside the final histogram, even though it appears to have a modest error, weighing the value with the one the final ensemble converges.

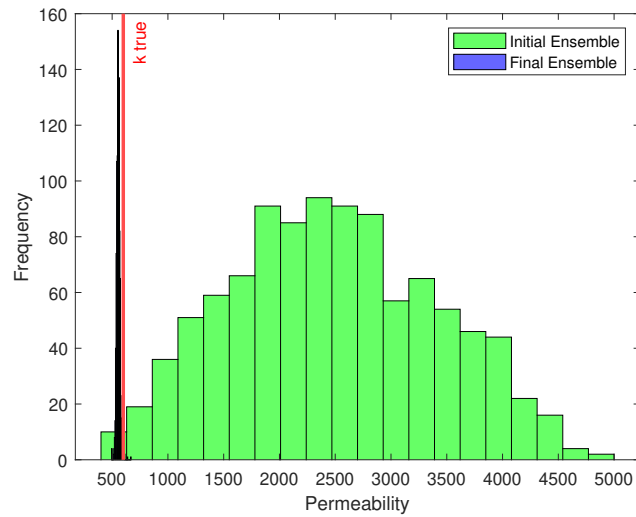


Figure 4.35: Permeability histogram on layer 1 for case D

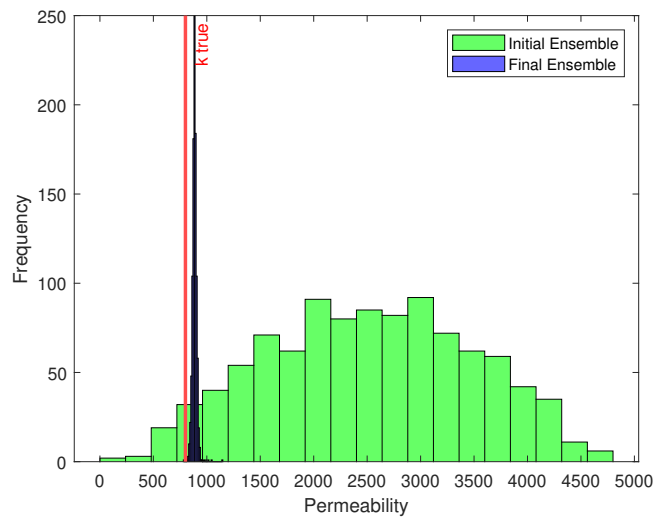


Figure 4.36: Permeability histogram on layer 2 for case D

Therefore, ES-MDA seems to have dealt well with case D and provided good results. Adding the flow-rate as observed data gives the impression of a good aid for stability for the final ensemble, a problem that appears on (SILVA et al., 2021).

## 5

### Conclusion and Future Works

In this thesis, we applied an analytical approach to an oil reservoir with an arbitrary number of layers in the Laplace domain using a piston-like water displacement to obtain a linear system concerning all layer and fluid properties, considering skin zone properties.

Solving the linear system obtained by the mathematical formulation, it was possible to calculate the pressure difference in the Laplace domain. Moreover, it was possible to obtain the flow-rate data deriving the pressure difference data quickly. Finally, using the Stehfest algorithm (STEHFEST, 1970), we could return to the actual domain and use them as input data for the static model.

We used the calculated flow-rate and pressure difference responses as input for the parameters estimation process. Here, we use the dimensionless ES-MDA due to the difference of magnitude in the input data vector. On the Dimensionless ES-MDA, we considered the vector of parameters to be evaluated as each layer permeability, skin zone radius, and skin zone permeability.

Also, an inflation factor analysis for the ES-MDA was considered, aiming to improve the static method's accuracy. Four cases were presented, testing the technique on different conditions, aiming to observe if changing some reservoir properties would not present good results in fitting the observed data and estimating the parameters.

The results were promising for all cases. Adding little information about the flow-rate and using the dimensionless ES-MDA improves the results presented on (SILVA et al., 2021), even when increasing the complexity and computing more parameters. For all cases, the actual value for all parameters is inside their final histogram. The data fitting for pressure difference and flow rate also worked for all situations, even for case D, in which (SILVA et al., 2021) had a problem fitting the pressure difference data. Therefore, the applied method met expectations for all cases, showing good convergence.

An idea for future work is to consider the complete relative permeability curve as in article (SILVA et al., 2021), not only a piston-like water displacement. One possible approach is to consider the entire relative permeability curve as an iterative of multiple piston-like water displacement. Another suggestion is to reflect on the possibility of cross-flow between each layer as in (VIANA et al., 2022), changing the construction of the linear system of the mathematical model. Both options increase the problem's complexity but are

closer to a more realistic situation.

## 6

### Bibliography

ABRAMOWITZ, M.; STEGUN, I. A. **Handbook of Mathematical Functions with Formulas, Graphs, and Mathematical Tables**. ninth dover printing, tenth gpo printing. New York: Dover, 1964.

BARLOW, R. J. **Statistics: A Guide to the Use of Statistical Methods in the Physical Sciences (Manchester Physics Series)**. Reprint. [S.l.]: Wiley-Blackwell, 1989. ISBN 0471922951.

BARRETO, A.; PERES, A.; PIRES, A. Water injectivity tests on multilayered oil reservoirs. **Society of Petroleum Engineers Brasil Offshore - Macaé, Brazil (2011-06-14)**, 2011.

BELA, R. V.; PESCO, S.; BARRETO, A. B. Impulse functions applied to compute pressure change during injectivity tests. **Fuel**, v. 310, p. 122392, 2022. ISSN 0016-2361. Disponível em: <<https://www.sciencedirect.com/science/article/pii/S001623612102264X>>.

BUCKLEY, S.; LEVERETT, M. Mechanism of Fluid Displacement in Sands. **Transactions of the AIME**, v. 146, n. 01, p. 107–116, 12 1942. ISSN 0081-1696. Disponível em: <<https://doi.org/10.2118/942107-G>>.

EMERICK, A. A.; REYNOLDS, A. C. Ensemble smoother with multiple data assimilation. **Computers & Geosciences**, v. 55, p. 3–15, 2013. ISSN 0098-3004. Ensemble Kalman filter for data assimilation. Disponível em: <<https://www.sciencedirect.com/science/article/pii/S0098300412000994>>.

EVENSEN, G. Sequential data assimilation with a nonlinear quasi-geostrophic model using monte carlo methods to forecast error statistics. **Journal of Geophysical Research: Oceans**, v. 99, n. C5, p. 10143–10162, 1994. Disponível em: <<https://agupubs.onlinelibrary.wiley.com/doi/abs/10.1029/94JC00572>>.

GROETSCH, C. **The theory of Tikhonov regularization for Fredholm equations of the first kind**. [S.l.: s.n.], 1984. 44 p.

HANKE, M. A regularizing levenberg - marquardt scheme, with applications to inverse groundwater filtration problems. **Inverse Problems**, IOP Publishing, v. 13, n. 1, p. 79–95, feb 1997. Disponível em: <<https://doi.org/10.1088/0266-5611/13/1/007>>.

IGLESIAS, M.; DAWSON, C. The regularizing levenberg-marquardt scheme for history matching of petroleum reservoirs,. **Computational Geosciences**, v. 17, 02 2013.

IGLESIAS, M. A. **Iterative regularization for ensemble data assimilation in reservoir models**. 2014.

LE, D. H.; EMERICK, A. A.; REYNOLDS, A. C. An Adaptive Ensemble Smoother With Multiple Data Assimilation for Assisted History Matching. **SPE Journal**, v. 21, n. 06, p. 2195–2207, 12 2016. ISSN 1086-055X. Disponível em: <<https://doi.org/10.2118/173214-PA>>.

LEEUWEN, P. J. van; EVENSEN, G. Data assimilation and inverse methods in terms of a probabilistic formulation. **Monthly Weather Review**, American Meteorological Society, Boston MA, USA, v. 124, n. 12, p. 2898 – 2913, 1996. Disponível em: <[https://journals.ametsoc.org/view/journals/mwre/124/12/1520-0493\\_1996\\_124\\_2898\\_daaimi\\_2\\_0\\_co\\_2.xml](https://journals.ametsoc.org/view/journals/mwre/124/12/1520-0493_1996_124_2898_daaimi_2_0_co_2.xml)>.

LEFKOVITS, H. et al. A Study of the Behavior of Bounded Reservoirs Composed of Stratified Layers. **Society of Petroleum Engineers Journal**, v. 1, n. 01, p. 43–58, 03 1961. ISSN 0197-7520. Disponível em: <<https://doi.org/10.2118/1329-G>>.

MASTBAUM, A. et al. Dual-phase flow in two-layer porous media: a radial composite laplace domain approximation. **Journal of Petroleum Exploration and Production Technology**, v. 11, 09 2021.

NETO, J. L. F. B. et al. Pressure behavior during injectivity tests - a composite reservoir approach. In: . [S.l.: s.n.], 2020.

NIE, R.-S. et al. New modelling of transient well test and rate decline analysis for a horizontal well in a multiple-zone reservoir. **Journal of Geophysics and Engineering**, v. 8, p. 464, 07 2011.

RAFIEE, J.; REYNOLDS, A. C. Theoretical and efficient practical procedures for the generation of inflation factors for ES-MDA. **Inverse Problems**, IOP Publishing, v. 33, n. 11, p. 115003, oct 2017. Disponível em: <<https://doi.org/10.1088/1361-6420/aa8cb2>>.

REYNOLDS, A. C.; ZAFARI, M.; LI, G. Iterative forms of the ensemble kalman filter. European Association of Geoscientists amp; Engineers, 2006. ISSN 2214-4609. Disponível em: <<https://www.earthdoc.org/content/papers/10.3997/2214-4609.201402496>>.

SILVA, T.; PESCO, S.; JR, A. B. Influences of the inflation factors generation in the main parameters of the ensemble smoother with multiple data assimilation. **Journal of Petroleum Science and Engineering**, v. 203, p. 108648, 03 2021.

SILVA, T. M. et al. Es-mds applied to estimate skin zone properties from injectivity tests data in multilayer reservoirs. **Computers & Geosciences**, v. 146, p. 104635, 2021. ISSN 0098-3004. Disponível em: <<https://www.sciencedirect.com/science/article/pii/S0098300420306130>>.

STEHFEST, H. Algorithm 368: Numerical inversion of laplace transforms. **Communications of the ACM**, 1970.

TARANTOLA, A. **Inverse Problem Theory and Methods for Model Parameter Estimation**. Society for Industrial and Applied Mathematics, 2005. Disponível em: <<https://epubs.siam.org/doi/abs/10.1137/1.9780898717921>>.

VIANA, I. et al. An analytical model for pressure behavior in multilayered radially composite reservoir with formation crossflow. **Journal of Petroleum Exploration and Production Technology**, 02 2022.

VOGEL, C. R. **Computational Methods for Inverse Problems**. Society for Industrial and Applied Mathematics, 2002. Disponível em: <<https://epubs.siam.org/doi/abs/10.1137/1.9780898717570>>.

ZHANG, F.; REYNOLDS, A.; OLIVER, D. Evaluation of the reduction in uncertainty obtained by conditioning a 3d stochastic channel to multiwell pressure data. **Mathematical Geology**, v. 34, p. 715–742, 08 2002.